

**NOAA NESDIS
CENTER FOR SATELLITE APPLICATIONS
AND RESEARCH**

Vegetation Index (VI) Product

**ALGORITHM THEORETICAL
BASIS DOCUMENT**

Version 2.1

NOAA NESDIS STAR

ALGORITHM THEORETICAL BASIS DOCUMENT

Version: 2.1

Date: May 18, 2021

TITLE: VIIRS VI Algorithm Theoretical Basis Document

Page 2 of 82

AUTHORS:

Corinne Carter (UMD/ ESSIC)

Mingshi Chen (IMSG)

Zhangyan Jiang (IMSG)

Yunyue Yu (STAR)

VI ALGORITHM THEORETICAL BASIS DOCUMENT VERSION HISTORY SUMMARY

Version	Description	Revised Sections	Date
1.0	New document creation	New Document	5/30/2019
2.0	Update to reflect algorithm changes and new validation work including work for validated maturity review	Throughout	8/26/2020
2.1	Update to reflect that current version of VI code is Version 3.0	1, 1.3, 3.1	

TABLE OF CONTENTS

	<u>Page</u>
LIST OF FIGURES	5
LIST OF TABLES	6
LIST OF ACRONYMS	8
ABSTRACT	10
1. INTRODUCTION	11
1.1 PURPOSE OF THIS DOCUMENT	12
1.2 WHO SHOULD USE THIS DOCUMENT	12
1.3 SUMMARY OF ALGORITHM CHANGES MADE SINCE VERSION 1	12
1.4 INSIDE EACH SECTION	13
2. VIIRS VI PRODUCTS OVERVIEW	14
2.2 INSTRUMENT CHARACTERISTICS	15
3. ALGORITHM DESCRIPTION	17
3.1 PROCESSING OUTLINE	17
3.2 ALGORITHM INPUT	29
3.2.1 VIIRS surface reflectance data	29
3.2.2 VIIRS TOA reflectance I1 data	30
3.2.3 VIIRS TOA reflectance I2 data	30
3.2.4 VIIRS geolocation data	30
3.2.5 VIIRS aerosol optical depth (AOD)	30
3.2.6 VIIRS cloud mask	30
3.2.7 MODIS land/water mask	31
3.3 THEORETICAL DESCRIPTION	31
3.3.1 Gridding	32
3.3.2 Reflectance aggregation	36
3.3.3 VI calculation	36
3.3.4 Compositing	37
3.3.5 VI QA assignment	43
3.4 ALGORITHM OUTPUT	47
3.5 PRACTICAL CONSIDERATIONS	53
3.5.1 Numerical computation consideration	53

NOAA NESDIS STAR

ALGORITHM THEORETICAL BASIS DOCUMENT

Version: 2.1

Date: May 18, 2021

TITLE: VIIRS VI Algorithm Theoretical Basis Document

Page 4 of 82

3.5.2	<i>Programming and procedural consideration</i>	54
3.5.3	<i>Quality assessment and diagnostics</i>	54
3.5.4	<i>Exception handling</i>	54
3.6	SAMPLE RESULTS	54
3.7	VALIDATION EFFORTS	58
3.7.1	<i>Validation strategy</i>	58
3.7.2	<i>Validation of VIIRS VI EDR granule product</i>	59
3.7.3	<i>Validation of VIIRS gridded and composited VI products</i>	63
4.	ASSUMPTIONS AND LIMITATIONS	76
4.1	ASSUMPTIONS	76
4.2	LIMITATIONS	76
5.	LIST OF REFERENCES	78

LIST OF FIGURES

	<u>Page</u>
Figure 1: Context level diagram showing input, main processing steps, and output for VI EDR production	18
Figure 2. Flow chart of VIIRS VI system.....	19
Figure 3. Unit level flowchart for daily gridding procedure for VI EDR production. a) Context including four individual threads. b) Processing performed within each thread.....	22
Figure 4. VI EDR aggregation unit level processing diagram. a) Overall input, processing, and output of aggregation process. b) Aggregation procedure carried out within each thread. ..	25
Figure 5. VIIRS VI block compositing unit processing. a) Overall processing scheme, including division into four parallel threads. b) Processing performed within each thread.	27
Figure 6. Unit level procedure diagram for block mosaicking.	28
Figure 7. Yearly mean sensor zenith angles and yearly mean percentage of forward scatter direction pixels of the maximum SAVI composited images over the tile H10V05 in 2007 as functions of the soil adjustment factor (L) values.....	38
Figure 8. Mean EVI composited by the maximum SAVI method using the five soil adjustment factor (L) values over the tile H10V05 in 2007.	39
Figure 9. Histograms of the sensor zenith angles composited by the traditional MVC based on NDVI (L=0) (a) and by the MVC based on SAVI (L=0.05) in different seasons (compositing periods beginning at DOYs 041, 121, 217 and 313) in 2007 over the tile H10V05.	40
Figure 10. C is designed as a function of the maximum SAVI.....	41
Figure 11. Comparison of the maximum value compositing and the maximum view angle adjusted SAVI compositing.	42
Figure 12. Histograms of sensor zenith angles composited by the MVA-SAVI method at different seasons.....	42
Figure 13: Flowchart for determining overall quality flag in an output VI grid cell	44
Figure 14. VIIRS VI browse images in the week of Oct 5-20, 2017. (a) VIIRS TOC global 0.036° 16-day composite EVI; (b) VIIRS TOC regional 0.009° 16-day composite EVI; (c) VIIRS TOA global 0.036° 16-day composite NDVI; (d) VIIRS TOA regional 0.009° 16-day composite NDVI; (e) VIIRS TOC global 0.036° 16-day composite NDVI; (f) VIIRS TOC regional 0.009° 16-day composite NDVI.	58
Figure 15. VIIRS TOA NDVI, TOC EVI and TOC NDVI Accuracy, Precision and Uncertainty (APU) are plotted as function of VIIRS VI values in global inter-comparison with MODIS VI.	60
Figure 16. VIIRS TOA NDVI, TOC EVI and TOC NDVI Accuracy, Precision and Uncertainty (APU) time series in global inter-comparison with MODIS VI.	61

Figure 17: Accuracy (red), precision (blue), and uncertainty (black) statistics for biweekly global NPP vs. NOAA20 vegetation index. (a), (b), and (c) are stratified by NPP VI value, with histograms of total numbers of pixels in each value bin shown in gray. (a) TOA NDVI. (b) TOC NDVI. (c) TOC EVI. (d), (e), and (f) show time series statistics. (d) TOA NDVI. (e) TOC NDVI. (f) TOC EVI. 68

Figure 18: Accuracy (red), precision (blue), and uncertainty (black) statistics for NOAA vs. NASA NPP VIIRS vegetation indices. (a) and (b) are stratified by NOAA VI value, with histograms of numbers of pixels shown in gray. (a) TOC NDVI. (b) TOC EVI. Time series are shown in (c) and (d). (c) TOC NDVI. (d) TOC EVI. 71

Figure 19: Accuracy (red), precision (blue), and uncertainty (black) statistics for biweekly global NPP VIIRS vs. MODIS vegetation indices. (a) and (b) are stratified by NOAA VI value, with histograms of numbers of pixels shown in gray. (a) TOC NDVI. (b) TOC EVI. Time series are shown in (c) and (d). (c) TOC NDVI. (d) TOC EVI. 73

Figure 20: Time series of June- December 2019 biweekly global NOAA20 TOA NDVI (red), TOC NDVI (green), and TOC EVI (blue) compared to PhenoCam GCC (black), for (a) CanadaOBS site, (b) mead2 site, (c) willowcreek site. 75

LIST OF TABLES

Table 1. Requirement of JPSS Vegetation Indices Product	14
Table 2. Summary of VIIRS VNIR and SWIR Spectral Band Characteristics	16
Table 3. Input Data of the VIIRS VI System	29
Table 4. Contents of intermediate 0.003° resolution gridded data file.	32
Table 5. Quality flags in 0.003 degree intermediate file	33
Table 6. Bit Layout of the Two QFs in the NVPS VI Product	46
Table 7. VIIRS VI Output Files	48
Table 8. VIIRS VI Output Files Standard Name Description	49
Table 9. Data Fields of the NVPS VI Product	50
Table 10. Metadata Information Example for the NVPS VI Product.....	52
Table 11. VIIRS VI EDR global APU estimation	62
Table 12. VIIRS VI EDR global APU estimation in comparison with MODIS VIs.....	63
Table 13. Overall statistics for NPP vs. NOAA20 vegetation indices.....	68
Table 14. Overall statistics for comparison of NOAA to NASA NPP VIIRS VIs.	71
Table 15. Overall statistics for NPP VIIRS vs. MODIS vegetation indices.	73

LIST OF ACRONYMS

ARVI	Atmospheric Resistant Vegetation Index
ATBD	Algorithm Theoretical Basis Document
CDR	Critical Design Review
DoD	Department of Defense
EVI	Enhanced Vegetation Index
ESSIC	Earth System Science Interdisciplinary Center
GVF	Green Vegetation Fraction
GVFP	Green Vegetation Fraction Product
GVPS	Global Vegetation Processing System
HDF	Hierarchical Data Format
IMSG	I. M. Systems Group
IP	Intermediate Product
JPSS	Joint Polar Satellite System Program
LAI	Leaf Area Index
L1RDS	Level 1 Requirements Supplement
NIR	Near Infrared
km	Kilometer
MB	Mega Byte
μm	Micron
MODIS	Moderate Resolution Imaging Spectroradiometer
MVC	Maximum Value Compositing
NASA	National Aeronautics and Space Administration
NCEP	National Center for Environmental Prediction
NDVI	Normalized Difference Vegetation Index
NESDIS	National Environmental Satellite, Data, and Information Service
NetCDF	Network Common Data Form
NIR	Near Infrared
NOAA	National Oceanic and Atmospheric Administration
OSPO	Office of Satellite and Product Operations
PDR	Preliminary Design Review
PNG	Portable Network Graphics
QA	Quality Assurance
RIP	Retained Intermediate Product

NOAA NESDIS STAR

ALGORITHM THEORETICAL BASIS DOCUMENT

Version: 2.1

Date: May 18, 2021

TITLE: VIIRS VI Algorithm Theoretical Basis Document

Page 9 of 82

SAVI	Soil Adjusted Vegetation Index
SEVIRI	Spinning Enhanced Visible and Infrared Imager
SNPP	Suomi National Polar-orbiting Partnership
SPSRB	Satellite Products and Services Review Board
STAR	Center for Satellite Applications and Research
TIFF	Tagged Image File Format
TOA	Top of Atmosphere
TOC	Top of Canopy
UMD	University of Maryland, College Park
USGS	United States Geological Survey
VHP	Vegetation Health Product
VIIRS	Visible Infrared Imager Radiometer Suite

ABSTRACT

This document is the Algorithm Theoretical Basis Document (ATBD) for the VIIRS Vegetation Index (VI) operational product system, developed by the NOAA/NESDIS Center for Satellite Applications and Research (STAR). The main function of the VI system is to produce Top of Atmosphere (TOA) Normalized Difference Vegetation Index (NDVI), Top of Canopy (TOC) NDVI and Top of Canopy Enhanced Vegetation Index (TOC EVI) from the Visible Infrared Imager Radiometer Suite (VIIRS) sensor onboard Suomi National Polar-orbiting Partnership (SNPP) and NOAA20 satellites. These products are intended for applications in numerical weather and seasonal climate prediction models at the National Centers for Environmental Prediction (NCEP). The retrieval algorithm uses VIIRS red (I1), near-infrared (I2) and blue (M3) bands centered at 0.640 μm , 0.865 μm and 0.490 μm , respectively, to calculate NDVI and EVI. This document describes the details of the VI algorithm that is used for VIIRS VI production. To meet the data needs of NCEP and other potential users, the VIIRS VI algorithm produces TOA NDVI, TOC NDVI, and TOC EVI in daily, daily rolling weekly (8-day) composite and daily rolling 16-day composites at 4-km resolution (global scale) and 1-km resolution (regional scale). Details of these products are presented in Sections 2 and 3 of this document. Some operational considerations are given in Section 4.

1. INTRODUCTION

Vegetation Index (VI) is a robust empirical measure of vegetation activity at the land surface, and has been widely used to study the spatial and temporal pattern of vegetation conditions at large scale with the objective to understand the role of terrestrial vegetation in regional and global processes, such as global carbon and nitrogen cycle, global hydrological cycle and global energy cycle. The MODerate Resolution Imaging Spectrometer (MODIS) Vegetation Indices (VIs) product represented the best available data source for studying large scale land surface vegetation dynamics in the last two decades.

On the heritage of the NOAA AVHRR and NASA EOS MODIS, the Visible Infrared Imager Radiometer Suite (VIIRS) onboard NASA's Suomi National Polar-orbiting Partnership (S-NPP) satellite instrument was successfully launched in Nov 21, 2011. The Suomi NPP VIIRS Vegetation Index Environment Data Record (VIIRS VI-EDR) product, built and expanded on the MODIS VI product, has become operational within the Suomi NPP Data Exploitation (NDE) production facility as of February 12, 2015. Gridded global and regional VIIRS VI EDR processing for NPP and NOAA20 became operational at NDE on June 4, 2019. The NDE is a production facility within the NOAA Environmental Satellite Processing Center (ESPC), which in turn is an element of the JPSS common ground segment.

The current version (Version 3.0) of S-NPP VIIRS Vegetation Index (VI) produces gridded VI product at global scale and North America-centric regional scale. The global gridded VI products are consistent with the already operational global SNPP and NOAA20 VIIRS Green Vegetation Fraction (GVF) product gridded at 4 km resolution. Meanwhile the North America-centric regional VI products, spanning from 7.5°S northward to the Pole, and from 130°E eastward to 30°E, are produced at 1 km resolution, consistent with the operational regional VIIRS GVF product.

Three VI products are made both globally and regionally over land regions: the Top of the Atmosphere (TOA) Normalized Difference Vegetation Index (NDVI), the Top of the Canopy (TOC) NDVI, the TOC Enhanced Vegetation Index (EVI). The products come with associated relevant quality flags (i.e., Land/water mask, cloud confidence, and aerosol loadings). These VI products are produced at temporal scales of daily, weekly and bi-weekly at spatial resolutions with sizes of 4 km (0.036°, global scale) and 1km (0.009°, regional scale).

The VI algorithm development was initiated by Dr. Marco Vargas, with the scientists and developers of the STAR VI team, currently led by Dr. Yunyue Yu. The Office of Satellite and

Product Operations (OSPO) are responsible for product data storage, accessibility and dissemination.

1.1 Purpose of This Document

The purpose of this document is to provide a detailed description of the algorithm employed to produce the VIIRS VI product. Specifically, the document introduces the inputs required to produce the VIIRS VI products. The VIIRS VI products include TOA NDVI, TOC NDVI and TOC EVI, and quality flags associated with these three VIIRS VI products.

1.2 Who Should Use This Document

The intended users of this document are project managers, product customers, product users, requirement reviewers and code reviewers.

Project managers, requirements reviewers and customers will use this document to determine that the desired products will be produced such that they match the specifications stated in the project requirements.

Product customers will use this document to better understand the VIIRS VI products, and to learn how to use the VIIRS VI products in an appropriate manner. Product customers may come from government agencies (e.g., NOAA/NESDIS, USGS EROS), scientific communities (e.g., Universities) or remote sensing industries.

This document was prepared by the STAR JPSS/VIIRS VI development team led by Dr. Yunyue Yu and in consultation with primary customers and data users. The responsible entity for bookkeeping, accessibility and distribution of this document is the Operational Products Development Branch (OPDB) of the NESDIS Center for Satellite Applications and Research (STAR) Satellite Meteorology and Climatology Division (SMCD).

1.3 Summary of algorithm changes made since Version 1

The following changes and improvements have been made to the VIIRS Vegetation Index algorithm since Version 1 of this ATBD and associated Version 1 code. (The changes listed below reflect the algorithm as implemented in the VI version 3.0 code.):

- Aggregation of 0.003° gridded data to the 0.036° global and 0.009° regional grids is performed before calculation of output vegetation indices and compositing.
- Weekly vegetation indices are composited from 8 daily aggregated vegetation indices. Biweekly vegetation indices are composited from 2 weekly aggregated vegetation indices. This allows for faster processing than in Version 1, in which weekly and biweekly VIs were calculated directly from high resolution data and the aggregation process had to be repeated.
- Some processing is performed in blocks, in order to take advantage of parallel processing capabilities. These blocks are mosaicked to produce the global and regional output.
- Changes have been made to the quality flag scheme, increasing the number of overall product quality flag levels and reducing the quality flag volume in the output data to 2 bytes per pixel from 4.

1.4 *Inside Each Section*

This document contains the following sections:

Section 1.0 - Introduction. Section 1 provides the purpose and intended users of the ATBD.

Section 2.0 - VI System Overview. Section 2 describes the products generated by the algorithm and the characteristics of the instruments that supply inputs to the algorithm.

Section 3.0 - Algorithm Description. Section 3 describes the algorithm, including a processing overview, input data, physical description, mathematical description, algorithm output, performance estimates, practical considerations, and validation.

Section 4.0 - Assumptions and Limitations. Section 4 states assumptions that were made in determining that the software system architecture as designed will meet the requirements, and states limitations that may impact on the system's ability to meet requirements.

Section 5.0 - List of References. Section 5 provides a list of references cited in the document.

2. VIIRS VI PRODUCTS OVERVIEW

2.1 Objectives of VIIRS Vegetation Index

The worth of an operational VIIRS VI product has already been fully proven with the heritage of the AVHRR Normalized Difference Vegetation Index (NDVI) product (e.g. Gutman, 1991; Myneni, et al., 1997a; Gutman & Ignatov, 1998; Wessels et al., 2004; Anyamba & Tucker, 2005) and MODIS NDVI and EVI products (e.g. Huete et al., 2002; Zhang et al., 2003; Huete et al., 2006; Sims et al., 2006; Lunetta et al., 2006; Jiang et al., 2008; Funk & Budde, 2009). To ensure continuous provision of VI data, The Suomi NPP VIIRS Vegetation Index Environmental Data Record (VIIRS VI-EDR) product has become operational within the Suomi NPP Data Exploitation (NDE) production facility as of February 12, 2015, and NPP and NOAA20 gridded VIIRS VI product generation became operational within NDE on June 4, 2019. The current version of VI products was developed to meet the requirements:

- 1) Replacement of the AVHRR Global Vegetation Processing System (GVPS) production of vegetation index;
- 2) Generation of gridded VI products for operational use. JPSS operational TOA and surface reflectance products are initially generated in granule level (at 375 meter and 750 meter resolution at nadir). If VI was generated directly from the granules, it could not be ingested into NOAA operational monitoring and decision making systems; gridded VI products are required instead.

Therefore, global and regional gridded VI products are generated for operational use by the NOAA National Centers for Environmental Prediction (NCEP).

In general, the VI product requirements are defined by the JPSS program level 1 requirements document (L1RD) and Level 1 Requirements Document Supplement (L1RDS, at https://www.jpss.noaa.gov/assets/pdfs/technical_documents/L1RDS.pdf), as shown in Table 1.

Table 1. Requirement of JPSS Vegetation Indices Product

EDR Attribute	Threshold	Objective
Vegetation Indices Applicable Conditions:		
1. Clear, land (not ocean), daytime only		
a. Horizontal Cell Size	1km (regional), 4km (global)	1km
b. Mapping Uncertainty, 3 Sigma	4 km	1 km

NOAA NESDIS STAR

ALGORITHM THEORETICAL BASIS DOCUMENT

Version: 2.1

Date: May 18, 2021

TITLE: VIIRS VI Algorithm Theoretical Basis Document

Page 15 of 82

c. Measurement Range		
1. NDVI _{TOA}	-1 to +1	NS
2. EVI (1)	-1 to +1	NS
3. NDVI _{TOC}	-1 to +1	NS
d. Measurement Accuracy - NDVI _{TOA} (2)	0.05 NDVI units	0.01 NDVI units
e. Measurement Precision - NDVI _{TOA} (2)	0.04 NDVI units	NS
f. Measurement Accuracy - EVI (2)	0.05 NDVI units	0.01 EVI units
g. Measurement Precision - EVI (2)	0.04 NDVI units	NS
h. Measurement Accuracy - NDVI _{TOC} (2)	0.05 NDVI units	0.03 NDVI units
i. Measurement Precision - NDVI _{TOC} (2)	0.04 NDVI units	NS
j. Refresh	At least 90% coverage of the globe every 24 hours (monthly average)	24 hrs
Notes:		
1. EVI can produce faulty values over snow, ice, and residual clouds (EVI > 1).		
2. Accuracy and precision performance will be verified and validated for an aggregated 4 km horizontal cell		

2.2 Instrument Characteristics

VIIRS is one of five instruments onboard the SNPP satellite that launched on Oct. 28, 2011. It was intended to be the product of a convergence between the Department of Defense (DoD), NOAA and the National Aeronautics and Space Administration (NASA) in the form of a single visible/infrared sensor capable of satisfying the needs of all three communities, as well as the research community beyond. As such, VIIRS required three key attributes: high spatial resolution with controlled growth off nadir; minimal production and operational cost; and a sufficient number of spectral bands to satisfy the requirements for generating accurate operational and scientific products. Calibration is performed onboard using a solar diffuser for short wavelengths and a blackbody source and deep space view for thermal wavelengths. The nominal altitude for the SNPP satellite is 824 km. The VIIRS scan will therefore extend to 56 degrees on either side of nadir. An additional VIIRS instrument was included on the NOAA-20 satellite that launched on November 18, 2017, and a third VIIRS instrument will fly on board the planned J02 satellite.

The positioning of the VIIRS Visible/Near Infrared (VNIR) and Short Wave Infrared (SWIR) spectral bands is summarized in table 2. There are nine moderate (M) resolution bands and

three imagery (I) resolution bands in the VNIR and SWIR spectral region. The nadir resolutions for the M and I bands are 750 m and 375 m, respectively. The VIIRS VI algorithms use the VIIRS bands I1, I2 and M3 as input data.

Table 2. Summary of VIIRS VNIR and SWIR Spectral Band Characteristics

Band Name	Center	Width* (microns)	Resolution (m)
M1	0.415	0.020	750
M2	0.445	0.020	750
M3	0.490	0.020	750
M4	0.555	0.020	750
I1	0.640	0.075	375
M5	0.673	0.021	750
I2	0.865	0.039	375
M7	0.865	0.039	750
M8	1.240	0.020	750
I3	1.610	0.060	375
M10	1.610	0.060	750
M11	2.250	0.050	750

*Full width half maximum (FWHM)

2.3 Retrieval Strategy

The basic retrieval strategy of the NVPS system is to produce VIIRS gridded Vegetation Index (VI) products from VIIRS observations. First, VIIRS TOA and TOC reflectance data are gridded to 0.003 degree resolution. The daily reflectances gridded at 0.003 degree resolution are aggregated to the 0.009 degree resolution regional grid and the 0.036 degree resolution global grid, VI values are calculated, and quality flags determined to produce the daily product. Eight days worth of daily regional and global VIs and quality flags are composited to generate each weekly (8-day) VI product. In turn, VI from two eight-day periods are composited to produce the biweekly (16-day) VI products. Daily, weekly, and biweekly VIs are all produced at both global and regional scales.

3. ALGORITHM DESCRIPTION

3.1 *Processing Outline*

This algorithm outline describes the VI algorithm as implemented in the Version 3.0 VI code. The NVPS system generates daily, daily rolling weekly (8-day) and daily rolling biweekly (16-day) composite vegetation index products through the following steps:

- Step 1: VIIRS swath TOA reflectance in bands I1 and I2, and TOC surface reflectance data in bands I1, I2, and M3 during a calendar day (0000 – 2400 UTC) are mapped to the native VI geographic grid (0.003 degree Plate Carrée projection) to produce gridded daily TOA reflectance and surface reflectance maps, respectively. Quality Assurance (QA) information, including land cover types, cloud confidences, aerosol optical thickness, and band data availabilities, is also determined at the 0.003 degree scale. If more than one pixel maps to the same 0.003 degree grid cell on the same day, one of those pixels is selected through a compositing process to be retained and the others are discarded.
- Step 2: Daily reflectance and QA information on the 0.003 degree grid are aggregated to two larger grids, the 0.009 degree resolution regional grid and the 0.036 degree resolution global grid. Vegetation indices are calculated from the aggregated TOA and TOC reflectances. TOA NDVI is calculated from the aggregated band I1 and I2 TOA reflectances. TOC NDVI and TOC EVI are calculated from the daily aggregated band I1, I2, and M3 surface reflectances. QA information of the native VI grids is aggregated to 0.009 degree and 0.036 degree resolutions by certain rules. The TOA NDVI, TOC NDVI and TOC EVI and the aggregated reflectance and QA are written into daily global and regional output files.
- Step 3: Eight daily global VI data sets are composited to generate the weekly (8-day) global VI values. Eight daily regional VI data sets are composited to generate the weekly regional VI values. Quality flags associated with each grid cell in the global and regional daily data are also composited to generate quality flags for both weekly VI EDRs. The global and regional weekly VI values are written into the weekly VI output product files.
- Step 4: For each biweekly (16 day) period, two sets of weekly global gridded VI values are composited to generate biweekly global VI values. Similarly, biweekly regional

gridded VI values are generated by compositing two sets of weekly regional VI values. Associated quality flags are also composited. The biweekly VI values are written into the biweekly global and regional VI EDRs.

A high level algorithm context diagram is shown in Figure 1 and more processing details are shown in Figure 2. Unit level processing diagrams are shown in Figures 3 through 6. Explanations of the diagrams are included below each one.

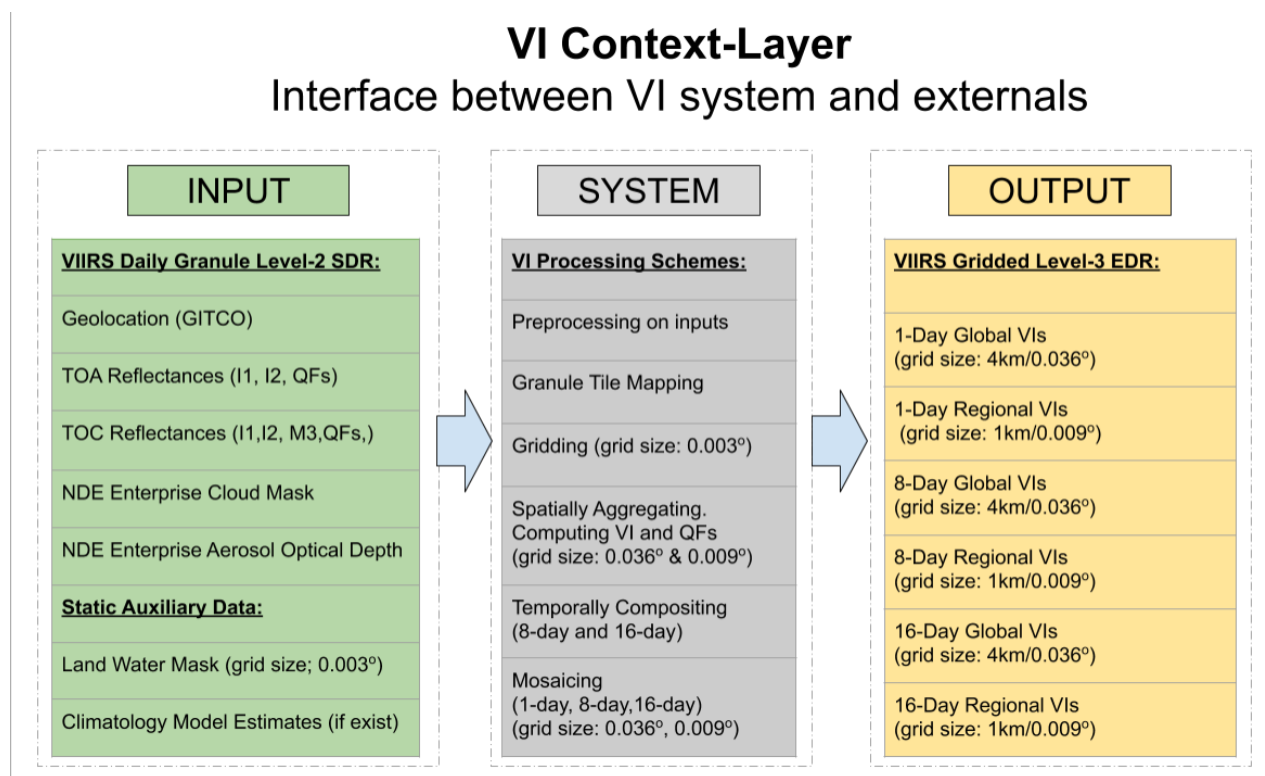


Figure 1: Context level diagram showing input, main processing steps, and output for VI EDR production

Figure 1 shows the overall scheme of input, processing, and output for VI EDR production. Inputs come from IDPS (reflectances and geolocation) and NDE (cloud mask and optical

depth.) Auxiliary land/ water mask and climatology estimates change infrequently so can be regarded as static. The processing steps are shown in general outline in the middle column of Figure 1. Each of these steps is described in more detail in Figures 2-6 below. The output of VIIRS EDR processing is shown in the third column in Figure 1. All VIs are produced at global and regional scales, and over 1, 8, and 16 day time intervals. All output is produced on a daily rolling basis, so for each day an 8-day product is produced including data from the previous 8 days, and a 16 day product is produced including data from the previous 16 days.

VI System Layer-- All Processes Flowchart

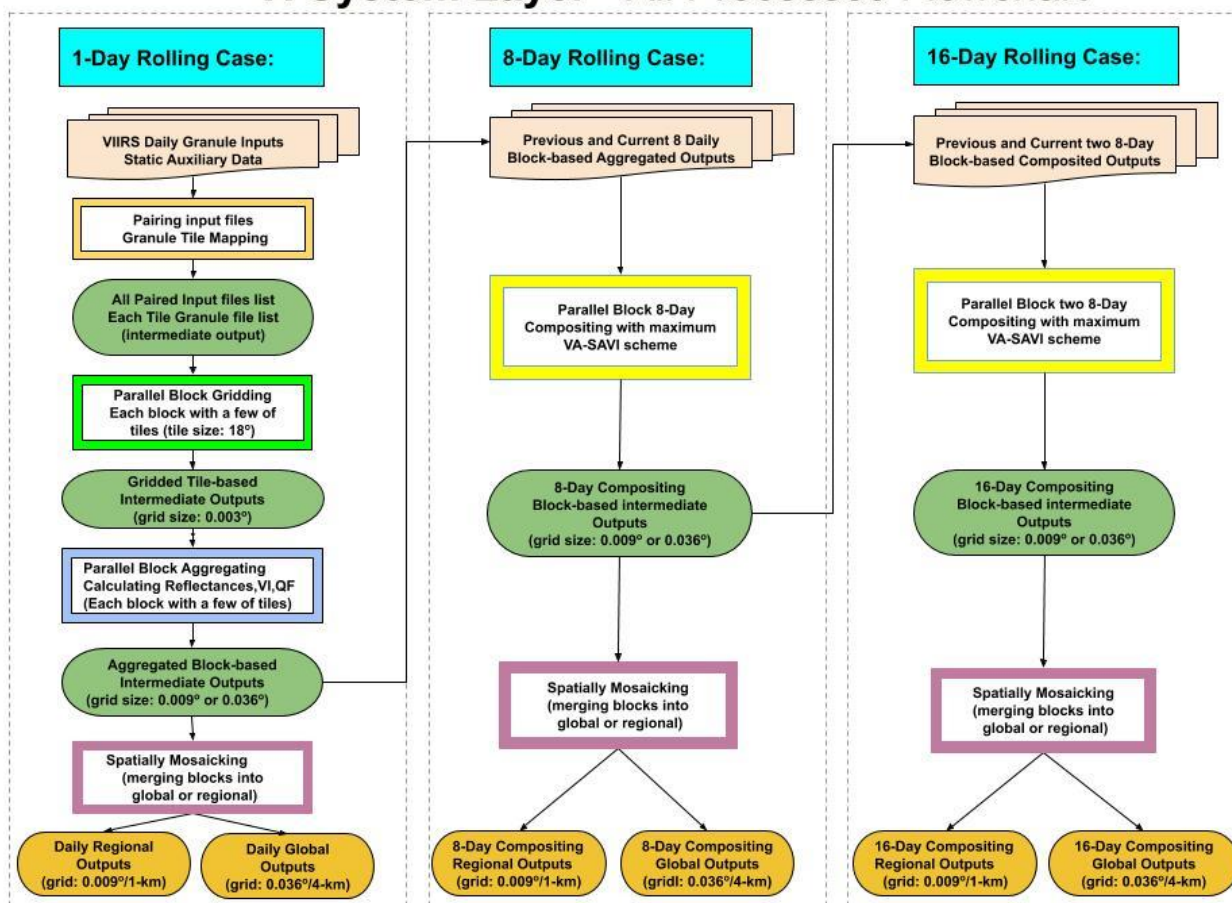


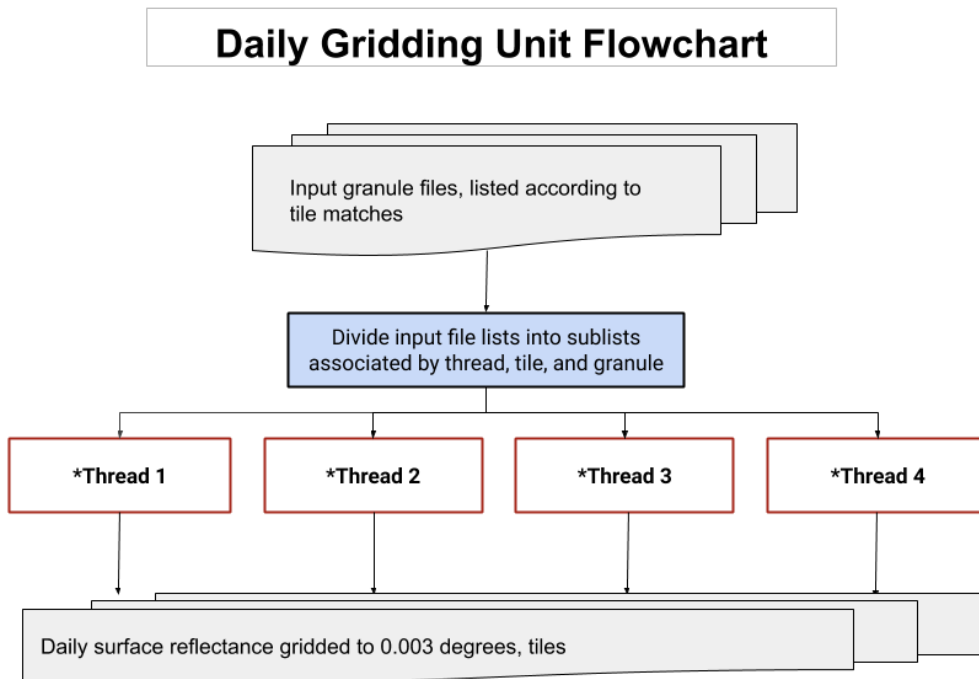
Figure 2. Flow chart of VIIRS VI system.

The first column of Figure 2 shows the process for generating the daily global and regional outputs. The input for this processing is the collection of TOA reflectance, surface reflectance, geolocation, cloud mask, and AOT granule data produced for one day. The different types of data are matched so that the different inputs that have a common observation time are put together. The geolocation from each granule is then used to determine which tiles the granule data will be mapped to. At this point groups of tiles are processed in blocks to reduce computing time through parallel processing, and this continues until spatial mosaicking immediately before output files are produced at the ends of the daily, weekly, and biweekly processing chains. Matching of granules to tiles is followed by performing the gridding of input granules for each tile. This gridding is done to the 0.003 degree grid. If more than one pixel from the same day maps to the same 0.003 degree grid cell, one of those pixels is selected through the VA-SAVI compositing method (described in Section 3.3.4). The data on the 0.003 degree grid are then aggregated to the 0.009 degree regional and 0.036 degree global grids. Only after this aggregation are vegetation indices calculated and quality flag values determined. The results of this aggregation are kept in blocks for input into the 8-day VI EDR process, and are also spatially mosaicked to be written out into the daily global and regional VI EDR files.

The middle column of Figure 2 shows the processing path to generate the weekly VI EDRs. The inputs to this processing are blocks of eight daily VI and quality flag data sets. The input data are kept in blocks in order not to exceed memory limits and to take advantage of parallel processing capabilities. For each grid cell in the global 0.036 degree and regional 0.09 degree grids, a compositing process is used to select data from one of the eight candidate days. The compositing process is described in detail in Section 3.3.4. Once compositing is completed for all blocks, they are kept as input to the 16-day VI EDR generation process, and also spatially joined together to produce the full global and regional output 8-day VI EDRs.

The right column of Figure 2 shows the procedure for generating the biweekly VI EDRs. Blocks of two weekly VI data sets are the input for each biweekly VI product. One of the two weekly VI and quality flag results is selected using the same compositing process as was used to generate the weekly VI composite from the daily gridded data. Since the biweekly VI processing takes its input from the weekly block data, it must then spatially mosaic the blocks to generate the full global and regional 16-day VI EDRs.

a)



b)

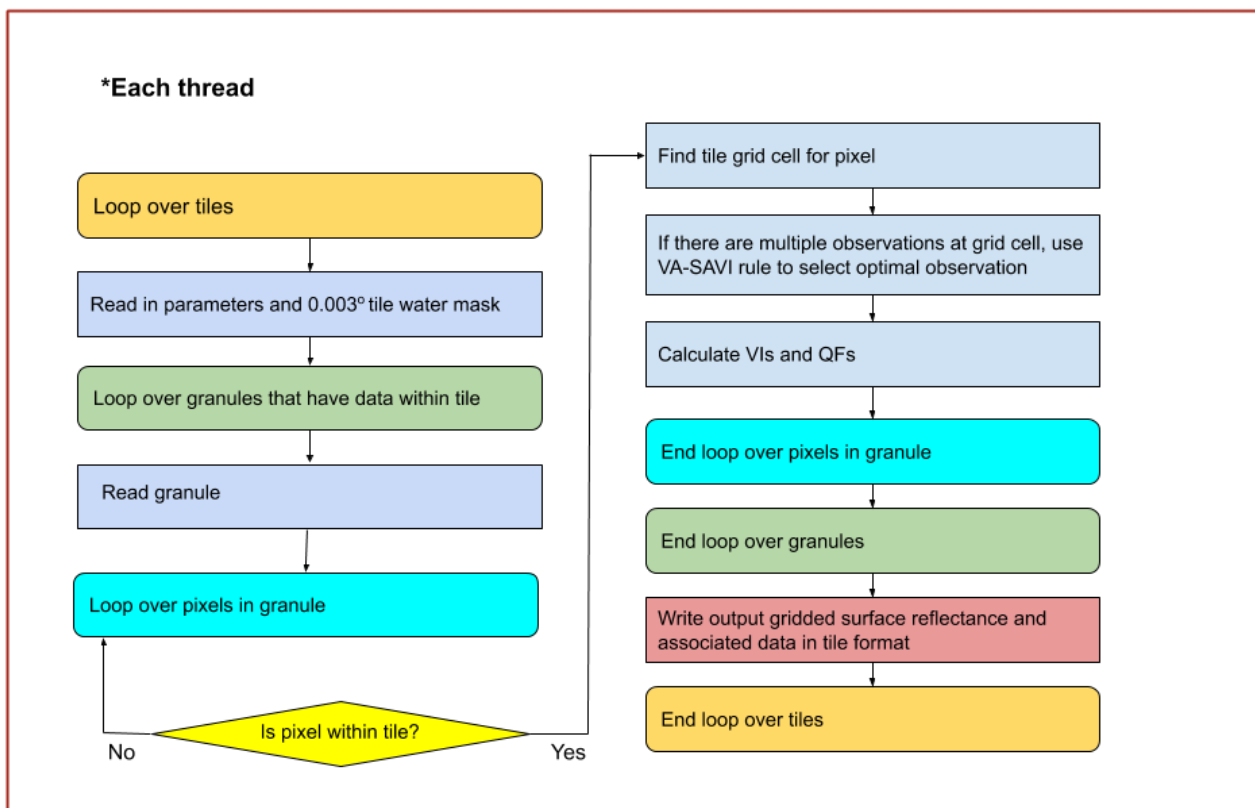


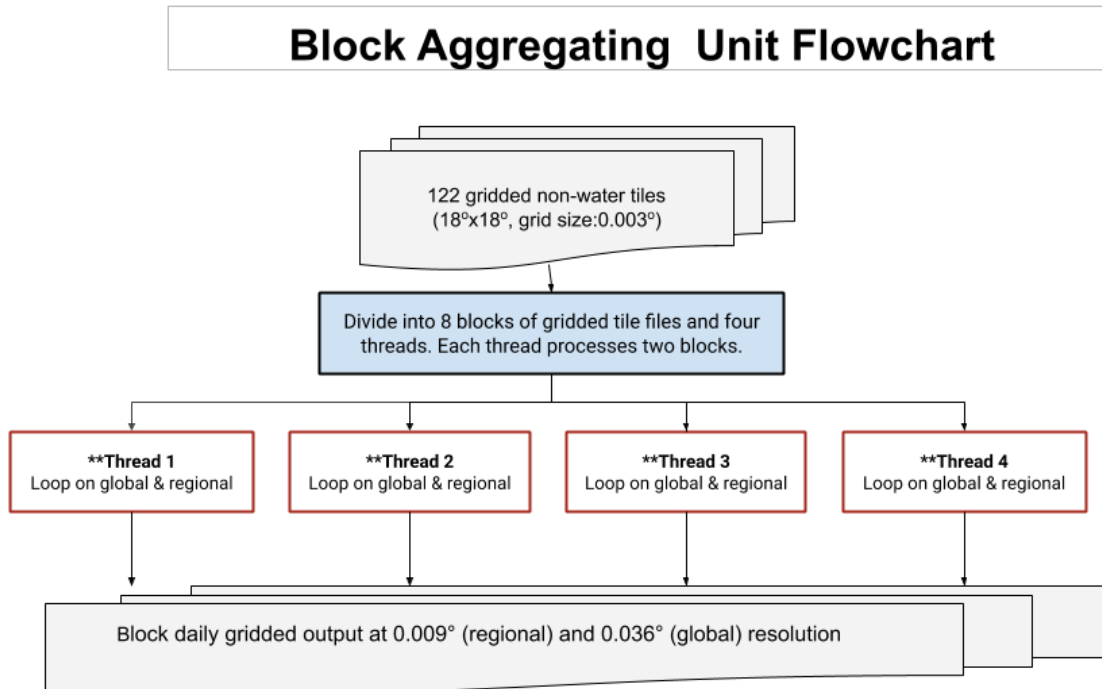
Figure 3. Unit level flowchart for daily gridding procedure for VI EDR production. a) Context including four individual threads. b) Processing performed within each thread.

Figure 3 shows the first major stage of VIIRS VI EDR production, the daily gridding. Figure 3-(a) shows the overall scheme of processing in the daily gridding unit. The input to the daily gridding unit is the set of granules representing a given day's data, and lists of the granules that correspond to each tile. These lists are divided into four groupings, which are processed by four parallel threads. The results of this processing are reflectances gridded

to $0.003^\circ \times 0.003^\circ$ resolution, with global coverage but separated into tiles for ease of processing.

Figure 3-(b) represents the processing performed by each of the threads in the daily gridding unit. Each thread processes a subset of the global set of tiles. Each granule that matches a tile has its pixel values projected onto that tile. Those pixels that fall within the tile are reprojected into the tile grid. If data from more than one granule falls within a tile grid cell, the VA-SAVI rule (described in Section 3.3.4 below) is used to select the data from one granule to keep; the others are discarded. Vegetation index and quality flag values are determined for each tile grid cell. Once all processing for a tile is complete, that tile is written out to be used in further processing. The data fields included in each tile are listed in Table 4 below. The quality flag scheme used at this stage of processing is described in Table 5.

a)



b)

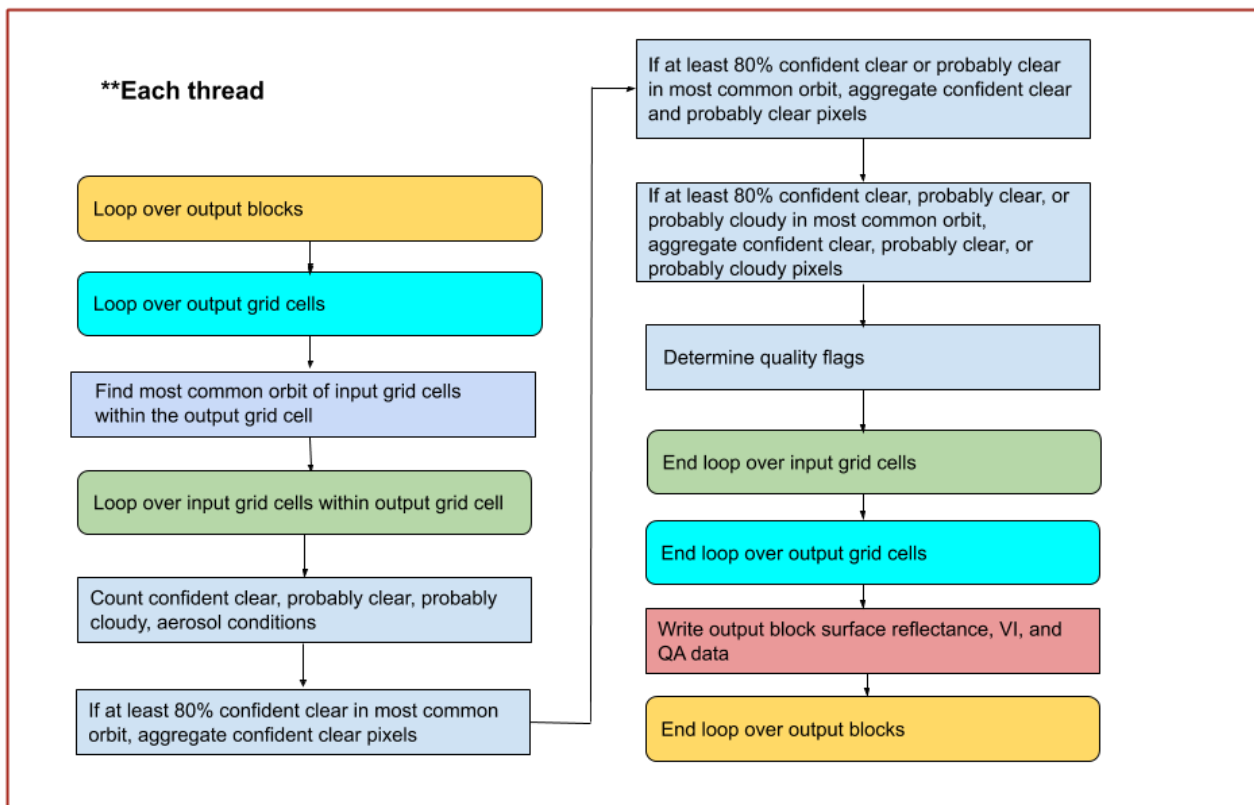
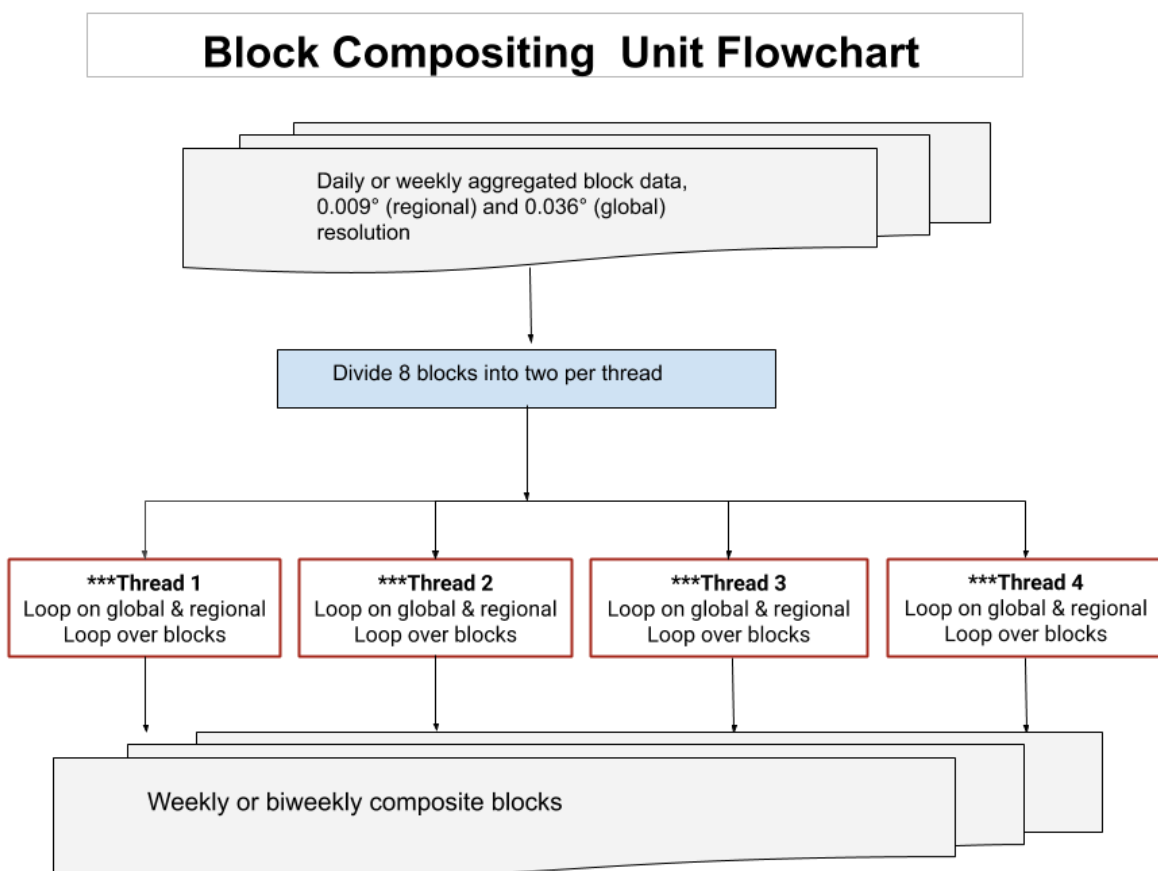


Figure 4. VI EDR aggregation unit level processing diagram. a) Overall input, processing, and output of aggregation process. b) Aggregation procedure carried out within each thread.

Figure 4 shows the unit level aggregation processing. This unit processes data from 0.003° resolution tile input into 0.009° and 0.032° block output. Figure 4-(a) shows that the input tiles are divided into eight groupings, with four parallel processing threads each processing two tile groupings. Each thread produces both global (0.032°) and regional (0.009°) grid tiles. Figure 4-(b) shows the procedure carried out within each thread. For each output grid cell, the most common orbit in its input grid cells is determined. The numbers of each of the possible cloud and aerosol conditions are counted among those grid cells from the most common orbit. If more than 80% of those pixels are confident clear, the confident clear

pixels are aggregated and the result labeled confident clear. Otherwise, if more than 80% of the pixels are confident clear or probably clear, those pixels are aggregated and the result labeled probably clear. Finally, if neither of the preceding two conditions is true but more than 80% of the pixels are confident clear, probably clear, or probably cloudy, those pixels are aggregated and the result labeled probably cloudy. Other quality flags are determined based on the logic described in Section 3.3.5. Vegetation indexes are calculated based on the aggregated reflectance values. Once aggregation is complete for all grid cells in a block, reflectances, vegetation indexes, and quality flags for that block are written to output for further processing.

a)



b)

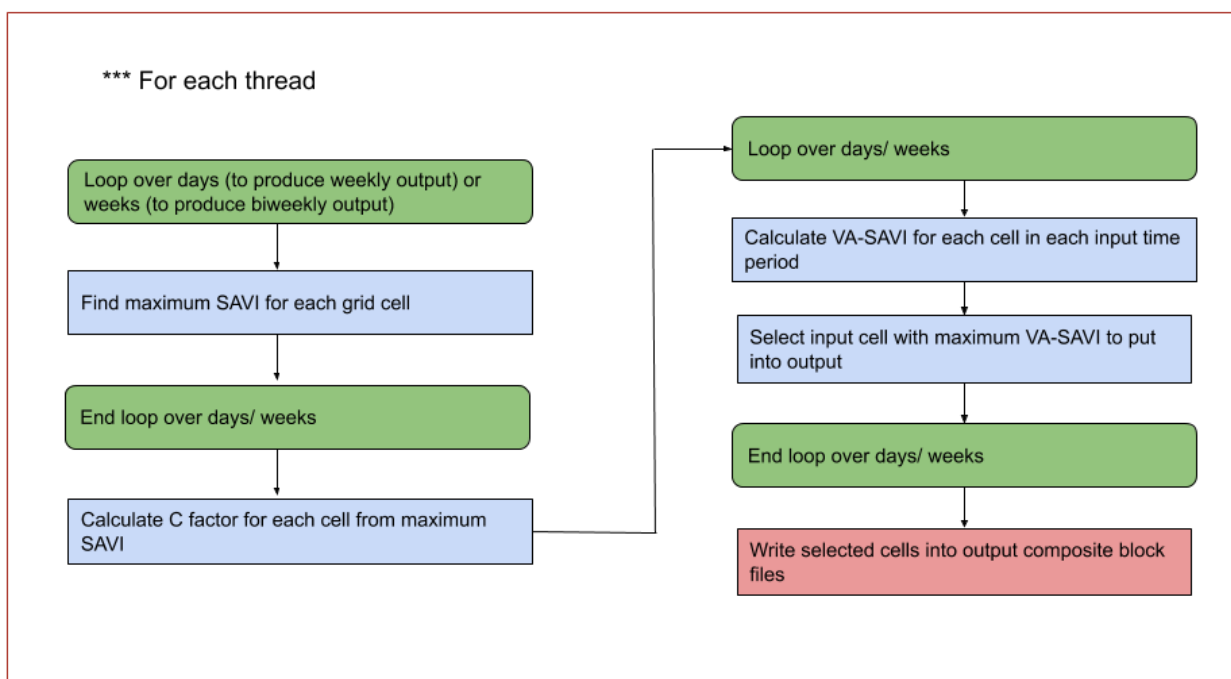


Figure 5. VIIRS VI block compositing unit processing. a) Overall processing scheme, including division into four parallel threads. b) Processing performed within each thread.

Figure 5 shows the unit level diagram for 8-day and 16-day compositing within VIIRS VI algorithm processing. Figure 5-(a) shows the overall procedure, including daily or 8-day block input, compositing processing in parallel, and 8- or 16-day block output. Eight input blocks are divided into two for each thread. Figure 5-(b) shows the compositing procedure within each thread. The loop over days (for 8-day output) or weeks (for 16-day output) is performed twice, first to obtain the maximum SAVI for each grid cell and from that the C factor for the VA-SAVI compositing formula, as described in Section 3.3.4. The second loop

over days or weeks is performed to apply the VA-SAVI formula and select one of the shorter time resolution input grid cells to be placed in the output grid cell. Once this is performed for all grid cells in a block, the composited block is written out for further processing. The 8-day composite blocks will be mosaicked to generate the global and regional 8-day VI EDRs (as shown in Figure 6), and will also be further composited to generate the 16-day composite blocks. The 16-day composite blocks will be mosaicked to generate the 16-day global and regional VI EDRs.

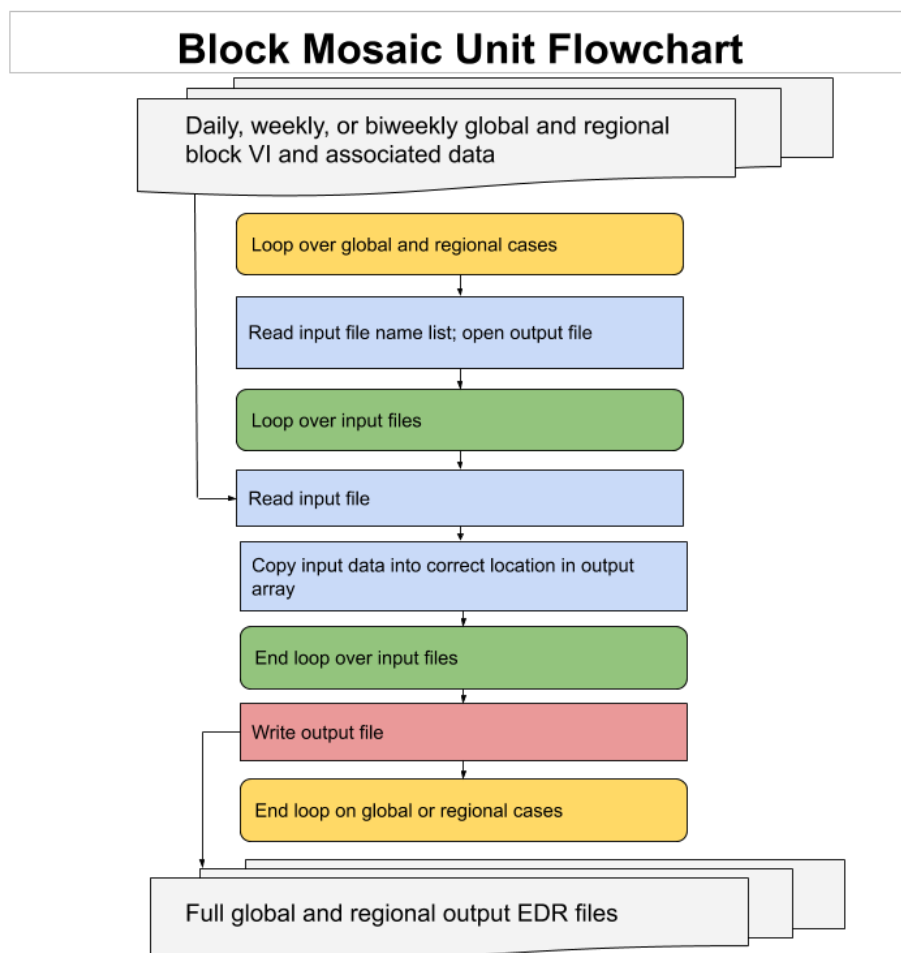


Figure 6. Unit level procedure diagram for block mosaicking.

Figure 6 shows the unit level procedure for performing mosaicking of blocks to generate global and regional VI EDRs. First, output memory is allocated. Input file names are read

from a list, then the input files themselves are read. The data from each input block is put into the correct location within the output memory. Once all input files have been read and copied, the data in the output memory are written into the output file. This procedure is repeated for global and regional products. This mosaicking is performed on daily, weekly, and biweekly block data.

3.2 Algorithm Input

The input data of the VIIRS VI system include the VIIRS TOC and TOA reflectance, geolocation, aerosol optical depth, cloud mask and land/water mask (table 3).

Table 3. Input Data of the VIIRS VI System

Name	File name	File format	Input type
VIIRS surface reflectance	SR	netCDF	Daily
VIIRS TOA reflectance I1 band	SVI01	HDF5	Daily
VIIRS TOA reflectance I2 band	SVI02	HDF5	Daily
VIIRS geolocation data	GITCO	HDF5	Daily
VIIRS aerosol optical depth	JRR-AOD	netCDF	Daily
Cloud mask	JRR-CloudMask	netCDF	Daily
MODIS land/water mask	MOD44W	HDF5	Static

3.2.1 VIIRS surface reflectance data

The VIIRS surface reflectance is a granule file (IVISR) that contains TOC reflectance data in the twelve VIIRS spectral bands listed in Table 2. The VI algorithm uses the red (I1), NIR (I2) and blue (M3) reflectance data to calculate the TOC NDVI and EVI. Cloud flag information is included in the IVISR files. Details of VIIRS surface reflectance RIP are available at https://www.star.nesdis.noaa.gov/jps/documents/ATBD/ATBD_SurfaceReflectance.pdf. The seven bytes of quality flag information included in the VIIRS surface reflectance (IVISR) files are described in the VIIRS Surface Reflectance External User's Manual (EUM) (NOAA STAR/ OSPO 2018)

3.2.2 VIIRS TOA reflectance I1 data

The VIIRS TOA surface reflectance I1 is a granule file (SVI01) that contains radiance, reflectance and quality flag data for the VIIRS I1 band. The VI algorithm uses the TOA I1 reflectance as red reflectance data to calculate TOA NDVI. Details of VIIRS sensor data record are available at https://www.star.nesdis.noaa.gov/jpss/documents/ATBD/D0001-M01-S01-003_JPSS_ATBD_VIIRS-SDR_D.pdf.

3.2.3 VIIRS TOA reflectance I2 data

The VIIRS TOA surface reflectance I2 is a granule file (SVI02) that contains radiance, reflectance and quality flag data for the VIIRS I2 band. The VI algorithm uses the TOA I2 reflectance as NIR reflectance data to calculate TOA NDVI. Details of VIIRS sensor data record are available at https://www.star.nesdis.noaa.gov/jpss/documents/ATBD/D0001-M01-S01-003_JPSS_ATBD_VIIRS-SDR_D.pdf

3.2.4 VIIRS geolocation data

The VIIRS geolocation files (GITCO) include latitude, longitude and sun-view geometry information corresponding to the VIIRS Surface Reflectance. The VI algorithm uses the latitude and longitude information in gridding and the sun-view geometry information in compositing. Further information about the VIIRS geolocation data is available at https://www.star.nesdis.noaa.gov/jpss/documents/ATBD/D0001-M01-S01-004_JPSS_ATBD_VIIRS-Geolocation_A.pdf

3.2.5 VIIRS aerosol optical depth (AOD)

JPSS Risk Reduction Unique Aerosol Optical Depth (JRR-AOD) data provides the aerosol optical depth at 550 nm. The VI algorithm reads the AOD Retrieval quality data and uses it in the quality assurance of the VIIRS VI products. Details of VIIRS AOD processing are available at https://www.star.nesdis.noaa.gov/jpss/documents/ATBD/ATBD_EPS_Aerosol_AOD_v3.0.1.pdf

3.2.6 VIIRS cloud mask

JPSS Risk Reduction Unique Cloud Mask (JRR-CloudMask) data provides the cloud mask of the VIIRS data. The VI algorithm reads the cloud mask data and uses it in the quality assurance of the VIIRS VI products. More information about the VIIRS cloud mask is available at https://www.star.nesdis.noaa.gov/jpss/documents/ATBD/ATBD_EPS_Cloud_Mask_v1.1.pdf

3.2.7 MODIS land/water mask

The Moderate Resolution Imaging Spectroradiometer (MODIS) 250-m land-water mask (MOD44W) was reprojected to the lat/lon projection and resampled to the VI grid resolution (see section 3.3.1). The land-water mask is used as a static input of the VI system to mask water pixels. Information about the MOD44W product is available at <https://lpdaac.usgs.gov/products/mod44wv006/>

3.3 *Theoretical Description*

Vegetation indices are spectral transformations of two or more bands designed to enhance the contribution of vegetation properties and allow reliable spatial and temporal inter-comparison of terrestrial photosynthetic activity and canopy structural variations (Huete et al., 2002). Although VIs are not intrinsic physical quantities, they are widely used as proxies in the assessment of many biophysical and biochemical variables, including canopy chlorophyll content (Blackburn, 1998; Gitelson et al., 2005), leaf area index (LAI) (e.g. Boegh et al., 2002; Chen & Cihlar, 1996), Green Vegetation Fraction (GVF) (e.g. ; Gutman & Ignatov, 1998; Jiang et al., 2006; Zeng et al., 2000), gross primary productivity (GPP) (Rahman et al., 2005; Sims et al., 2006), and fraction of photosynthetically active radiation absorbed by the vegetation (FAPAR) (e.g. Myneni et al., 1997b; Di Bella et al., 2004; Baret et al., 2007).

Normalized difference vegetation index (NDVI) time series data products based on the Advanced Very High Resolution Radiometer (AVHRR) instruments, such as the GIMMS (Global Inventory Modeling and Mapping Studies) and Pathfinder AVHRR Land (PAL) datasets, are available from 1981 onwards, and have contributed significantly to global land processes studies, vegetation–climate interactions, and other advancements in Earth System Science (e.g. Defries & Belward, 2000; Suzuki et al., 2007; Townshend, 1994; Tucker et al., 1986). The main disadvantages of the NDVI include the sensitivity to the variation of soil background (Huete, 1988), the inherent nonlinearity of ratio-based indices (Huete et al, 2002; Jiang et al, 2006) and the influence of atmospheric path radiances .

EVI was developed to optimize the vegetation signal with improved sensitivity in high biomass regions and improved vegetation monitoring through a de-coupling of the canopy background signal and a reduction in atmosphere influences (Huete et al, 2002). EVI has been used in a wide variety studies, including those on land cover/land use change (Wardlow et al., 2007), estimation of vegetation biophysical parameters (Chen et al., 2004; Houborg et al., 2007), phenology (Ahl et al., 2006; Xiao et al., 2006; Zhang et al., 2003),

evapotranspiration (Nagler et al., 2005), biodiversity (Waring et al., 2006), and the estimation of gross primary production (GPP) (Rahman et al., 2005; Sims et al., 2008, 2006).

EVI not only gains its heritage from the soil-adjusted vegetation index (SAVI) (Huete, 1988) and the atmospherically resistant vegetation index (ARVI) (Kaufman and Tanré, 1992), but also improves the linearity with vegetation biophysical parameters, encompassing a broader range in leaf area index (LAI) retrievals (Houborg et al., 2007). It has been shown to be strongly linearly related and highly synchronized with seasonal tower photosynthesis measurements in terms of phase and amplitude, with no apparent saturation observed over temperate evergreen needleleaf forests (Xiao et al., 2004), tropical broadleaf evergreen rainforests (Huete et al., 2006), and particularly temperate broadleaf deciduous forests (Rahman et al., 2005; Sims et al., 2006).

3.3.1 Gridding

The VI algorithm starts from VIIRS TOA and TOC reflectance granules and grids the data, using the nearest-neighbor method, onto a global 0.003° (333-m) grid. This grid is based on the Plate Carrée map projection and consists of 120,000×60,000 grid points (pixels) in the global map, which spans from 90° (north edge) to -90° (south edge) in the latitude and from -180° (west) to 180° (east) in longitude directions. If more than one pixel maps to the same 0.003° grid cell on the same day, one of those pixels is selected through the VA-SAVI compositing method as described in Section 3.3.4 below and kept for further processing. Vegetation index values are computed at each grid cell according to equations 3.4 and 3.5 below, and this information stored in the gridded intermediate file for research purposes. (The vegetation index values calculated here will not be included in the EDR output.) This gridded file is written out as an intermediate file in HDF5 format, in 6000 x 6000 grid cell tiles. The data fields and quality flag information contained in this intermediate file are described in Tables 4 and 5.

Table 4. Contents of intermediate 0.003° resolution gridded data file.

Variable name	Type	Description
DOY	int16	Day of year
I1_TOA	int16	Band I1 TOA reflectance
I2_TOA	int16	Band I2 TOA reflectance
I1_TOC	int16	Band I1 TOC reflectance
I2_TOC	int16	Band I2 TOC reflectance

NOAA NESDIS STAR

ALGORITHM THEORETICAL BASIS DOCUMENT

Version: 2.1

Date: May 18, 2021

TITLE: VIIRS VI Algorithm Theoretical Basis Document

Page 33 of 82

M3_TOC	int16	Band M3 TOC reflectance
NDVI_TOA	int16	Top of atmosphere NDVI
NDVI_TOC	int16	Top of canopy NDVI
EVI_TOC	int16	Top of canopy EVI
QF1	uint8	Quality flags byte 1 (See Table 5)
QF2	uint8	Quality flags byte 2 (See Table 5)
QF3	uint8	Quality flags byte 3 (See Table 5)
QF4	uint8	Quality flags byte 4 (See Table 5)
RAA	int16	Relative azimuth angle
SZA	int16	Solar zenith angle
VZA	int16	View zenith angle
ORBITID	Int16	Orbit ID number

Table 5. Quality flags in 0.003 degree intermediate file. Flags are listed in order from least significant bits (starting at 0) to most significant bits (ending at 7) in each byte. (Not all quality flags are used. This ATBD will be updated to indicate which flags in the intermediate file are set and used.)

Quality flag byte	Quality flag	Bits	Definitions
QF1	TOA NDVI quality	0	0 = good quality 1 = poor quality
	TOC EVI quality	1	0 = good quality 1 = poor quality
	TOC NDVI quality	2	0 = good quality 1 = poor quality
	Band I1 TOA reflectance quality	3	0 = good quality 1 = poor quality
	Band I2 TOA reflectance quality	4	0 = good quality 1 = poor quality

NOAA NESDIS STAR

ALGORITHM THEORETICAL BASIS DOCUMENT

Version: 2.1

Date: May 18, 2021

TITLE: VIIRS VI Algorithm Theoretical Basis Document

Page 34 of 82

	Band I1 TOC reflectance quality	5	0 = good quality 1 = poor quality
	Band I2 TOC reflectance quality	6	0 = good quality 1 = poor quality
	Band M3 TOC reflectance quality	7	0 = good quality 1 = poor quality
QF2	EVI out of range	0	0 = in range 1 = out of range
	Surface type	1-3	000 = desert 001 = land, not desert 010 = inland water 011 = sea water 101 = coastal
	Cloud confidence	4-5	00 = confident clear 01 = probably clear 10 = probably cloudy 11 = confident cloudy
	Sun glint	6	0 = no sun glint 1 = sun glint
	Spare	7	
QF3	Thin cirrus reflective	0	0 = thin cirrus 1 = no thin cirrus

NOAA NESDIS STAR

ALGORITHM THEORETICAL BASIS DOCUMENT

Version: 2.1

Date: May 18, 2021

TITLE: VIIRS VI Algorithm Theoretical Basis Document

Page 35 of 82

	Solar zenith angle stratification	1	0 = no stratification 1 = stratification
	AOT exclusion	2	0 = no exclusion 1 = exclusion
	Solar zenith angle exclusion	3	0 = no exclusion 1 = exclusion
	Snow	4	0 = no snow 1 = snow
	Adjacent cloud	5	0 = no adjacent cloud 1 = adjacent cloud
	Aerosol quantity	6-7	00 = climatology 01 = low 10 = average 11 = hiigh
QF4	Cloud shadow	0	0 = no shadow 1 = shadow
	Aerosol optical thickness quality	1-2	00 = high quality 01 = degraded quality 10 = excluded quality 11 = not produced
	Cloud mask quality	3-4	00 = poor 01 = low 10 = medium 11 = high
	Spare	5-7	

3.3.2 Reflectance aggregation

The daily gridded reflectance TOA and TOC reflectance data at the 0.003° grid are aggregated 3x3 to a 0.009° grid (~ 1 km) based on the spatial average method. The daily gridded TOA and TOC reflectance at the 0.003° grid are also aggregated 12x12 to a 0.036° grid (~ 4 km) based on the spatial average method. Not all pixels in the 3x3 or 12x12 aggregation areas are included in the average. The pixels to be included in the aggregation are determined as described in the quality flag processing section below (Section 3.3.5).

3.3.3 VI calculation

TOA NDVI is calculated using the aggregated TOA reflectance and TOC NDVI is calculated using the aggregated TOC reflectance at 1-km and 4-km resolutions respectively.

$$NDVI = \frac{\rho_{NIR} - \rho_{red}}{\rho_{NIR} + \rho_{red}} \quad (3.1)$$

TOC EVI is calculated using the aggregated TOC reflectance at 1-km and 4-km resolutions

$$EVI = G \frac{\rho_{NIR} - \rho_{red}}{\rho_{NIR} + C_1 \rho_{red} - C_2 \rho_{blue} + L} \quad (3.2)$$

where ρ_{NIR} , ρ_{red} , ρ_{blue} are the TOC NIR, red and blue reflectances respectively, L is the canopy background adjustment that addresses nonlinear, differential NIR and red radiant transfer through a canopy, and C1 and C2 are the coefficients of the aerosol resistance term, which uses the blue band to correct for aerosol influences in the red band. The coefficients adopted in the EVI algorithm are, L=1, C1=6, C2 = 7.5, and G (gain factor) = 2.5 (Huete, et al., 2002; Liu and Huete, 1995).

Due to the use of blue band, the denominator of the EVI equation could be equal to, or very close to, 0 and EVI values are abnormal under certain circumstance. For example, when ρ_{red} = 0.2380, ρ_{NIR} = 0.2255 and ρ_{blue} = 0.3538, the EVI value becomes infinite. A two-band EVI (EVI2) without a blue was developed by Jiang et al. (2008), which is robust under any circumstance and has the best similarity with the 3-band EVI.

$$EVI2 = 2.5 \frac{\rho_{NIR} - \rho_{red}}{\rho_{NIR} + 2.4 \rho_{red} + 1} \quad (3.3)$$

If the red/blue ratio is less than 1.25, or the blue reflectance is larger than 0.3, or EVI is larger than 0.7 or smaller than 0, then the EVI values are replaced by EVI2 values calculated using Eq. (3.6).

The results of the daily reflectance aggregation and VI calculations are written out into netCDF format intermediate files in blocks in order to facilitate parallel processing of the downstream 8- and 16- day products. The intermediate block data and quality flag fields are identical to the output data and quality flag fields except for field dimensions. The aggregated reflectance and calculated VI are also geographically mosaicked to produce the full global and regional vegetation index, reflectance, quality assurance, and sun/ view angles, which are written out in netCDF format as the daily global and regional VI EDRs.

3.3.4 Compositing

The VI algorithm input includes the VIIRS TOA and TOC reflectance and geolocation data for each granule. Daily VI are computed from daily aggregated TOA and TOC reflectances. Daily vegetation index data in an 8-day period are composited daily (daily rolling weekly). Eight-day vegetation index data are composited every day to produce a daily rolling biweekly (16 day) VI product. A daily rolling 8- or 16-day compositing period can start at any day of a year and covers 8 or 16 days. The next compositing period shifts one day after the last 8-day or 16-day period. At the end of a year, a compositing period covers some days in the next year if there are not enough days left in the year. The end result of compositing over an 8-day or 16-day period is a single file containing, for each 0.009 or 0.036 degree grid point, TOA NDVI, TOC NDVI, TOC EVI, TOA and TOC red (I1) and NIR (I2) reflectance, TOC blue (M3) reflectance, sensor and solar zenith angles, relative azimuth angle, and quality flags in a netCDF file.

The compositing procedure developed for the NOAA VIIRS GVF system is adopted in the VIIRS VI system, which is different from the traditional maximum value compositing (MVC) procedure used in the GVPS system. It is well documented that MVC based on NDVI favors observations in the forward scatter direction, creating a bias and resulting in low red and NIR reflectances because of shadowing effect (Cabral et al., 2003; Carreiras et al., 2003; van Leeuwen et al., 1999; Stoms et al., 1997; Cihlar et al., 1994; Huete et al., 1992; Gutman, 1991). To reduce the bias, the soil-adjusted vegetation index (SAVI), with varying soil adjustment factor (L) values, is proposed and tested for MVC using the MYD09GA data (i.e. VIIRS surface reflectance proxy data). It was found that L had great impact on the selection of the composited data. With the increase of the L value from 0 to 0.5, the bias shifted from the forward scatter direction to the backscatter direction (Figure 7). Mean EVI values

composited based on SAVI are greater than those composited based on NDVI (L=0) (Figure 8). The SAVI with L=0.05 was found to be the optimal vegetation index used in compositing to minimize the bias between the two directions (Figure 7).

$$SAVI = (1 + L) \frac{\rho_{NIR} - \rho_{red}}{\rho_{NIR} + \rho_{red} + L} \quad (3.4)$$

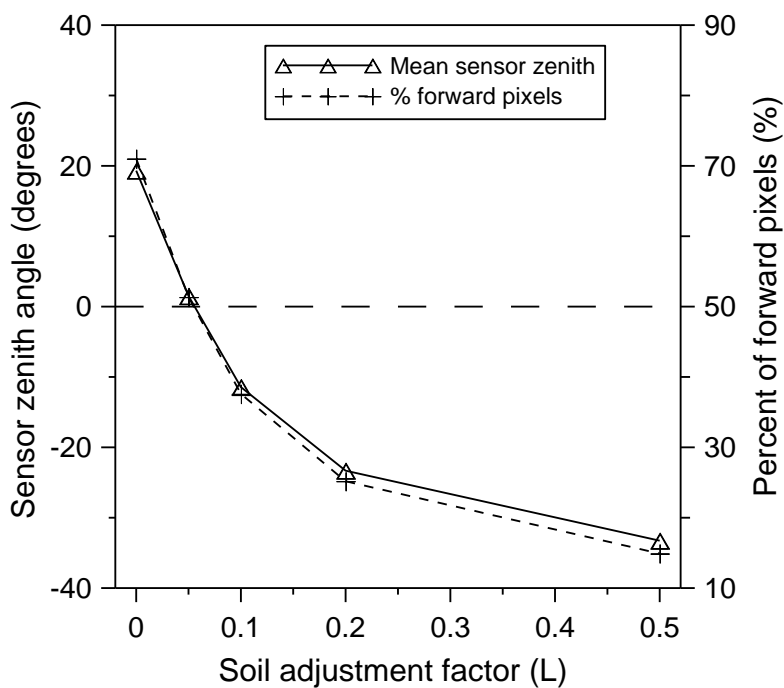


Figure 7. Yearly mean sensor zenith angles and yearly mean percentage of forward scatter direction pixels of the maximum SAVI composited images over the tile H10V05 in 2007 as functions of the soil adjustment factor (L) values.

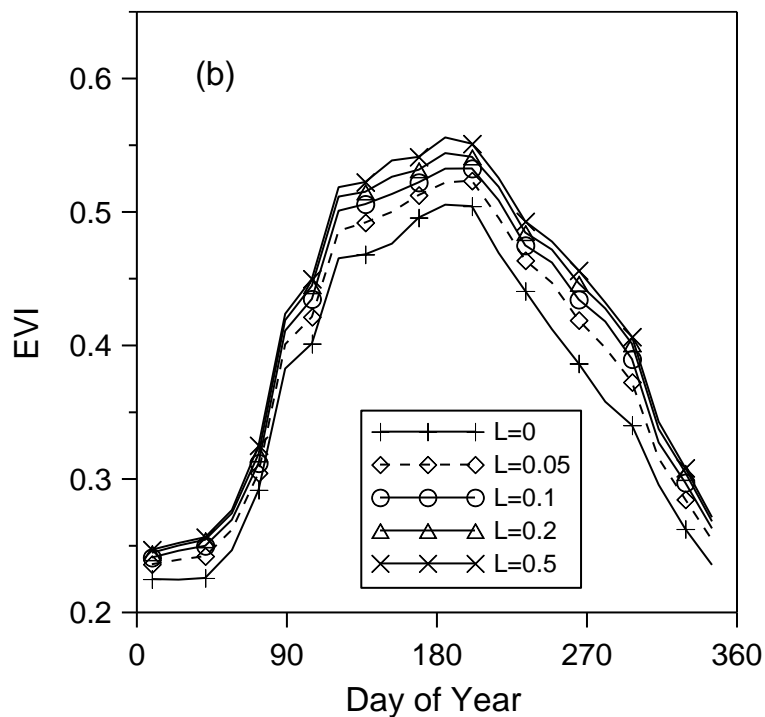


Figure 8. Mean EVI composited by the maximum SAVI method using the five soil adjustment factor (L) values over the tile H10V05 in 2007.

Although the bias in the view angle directions can be successfully minimized by the MVC based on SAVI ($L=0.05$), most of pixels composited by MVC are from high sensor zenith angles, regardless of whatever L values are used in compositing (Figure 9). In some cases, the maximum NDVI is selected at the expense of optimal view geometry since sensor zenith angles selected by MVC are often further off-nadir than necessary to ensure cloud-free viewing (Stoms et al, 1997). This is an inherent limitation of MVC since more vegetation canopies and fewer gaps among canopies can be observed from high view zenith angles than from the nadir view.

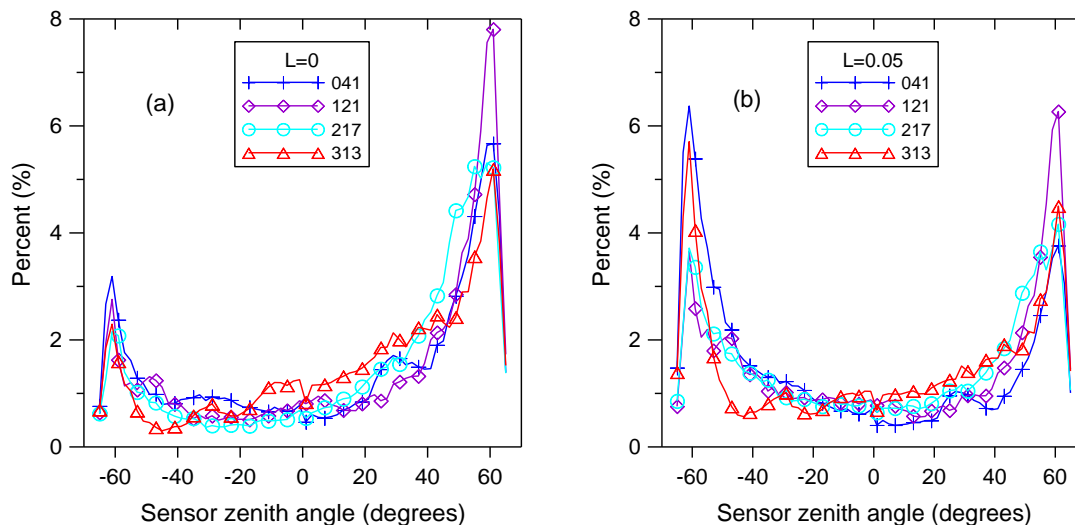


Figure 9. Histograms of the sensor zenith angles composited by the traditional MVC based on NDVI ($L=0$) (a) and by the MVC based on SAVI ($L=0.05$) in different seasons (compositing periods beginning at DOYs 041, 121, 217 and 313) in 2007 over the tile H10V05.

Thus, sensor zenith angles should be taken into account in compositing such that observations close to the nadir view are given a priority under clear sky conditions and observations at off-nadir view should be selected only if nadir view observations are cloudy. So, in compositing, SAVI should be adjusted according to the sensor zenith angle for each observation. The view-angle adjusted SAVI (VA-SAVI) is

$$\text{VA-SAVI} = \text{SAVI} - C \times \text{SZ}^2 \quad (3.5)$$

where SZ is the sensor zenith angle in degrees and C is a coefficient that accounts for the view angle variation of SAVI. The view angle variation of SAVI and other VIs is associated with the bidirectional reflectance distribution function (BRDF) of the surface. The BRDF effects are prominent over heterogeneous surfaces with intermediate vegetation density and insignificant over homogeneous surfaces, such as bare soil or fully vegetated area. So C is a function of vegetation density, which can be estimated by the maximum SAVI (SAVI_{\max}) in a compositing period for a pixel.

$$C = C_1 - C_2(\text{SAVI}_{\max} - 0.5)^2 \quad (3.6)$$

where $C_1=0.00008$ and $C_2=0.0002$. The C value is highest (0.00008) when $\text{SAVI}_{\max}=0.5$ and becomes 0.3 when $\text{SAVI}_{\max}=1$ or 0 (Figure 10). It should be noted that the C values are very small because the unit of sensor zenith angles in Eq. 3.6 is the degree.

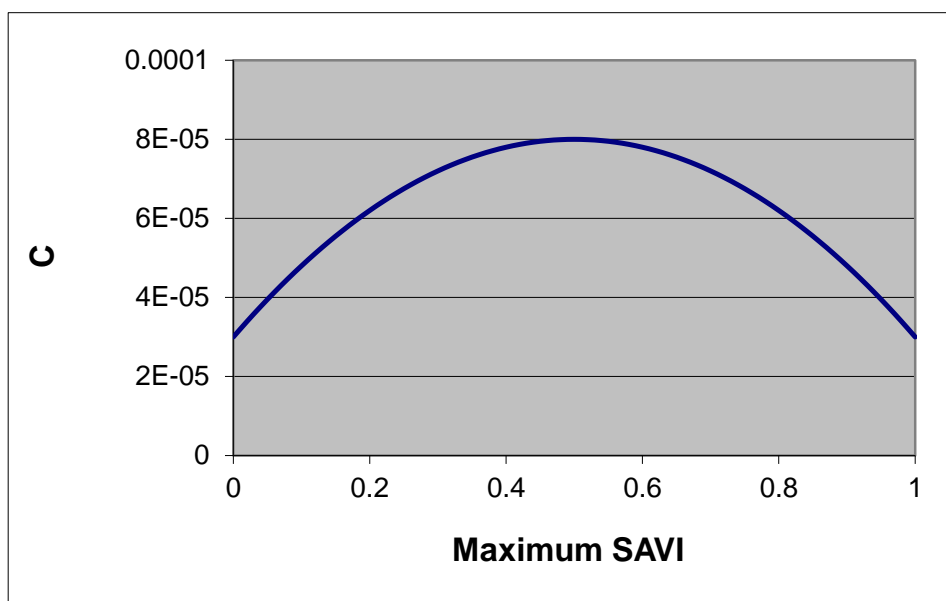


Figure 10. C is designed as a function of the maximum SAVI.

Instead of selecting the maximum NDVI, the VI compositing algorithm selects the maximum view-angle adjusted SAVI (MVA-SAVI) in a compositing period for each pixel. Figure 11 shows an example of the MVA-SAVI compositing, compared with the traditional MVC. In the compositing period, only one day of observation is cloudy and the other six days are cloud-free. MVC selects the maximum NDVI observation at sensor zenith angle 52° in the forward scatter direction. However, the MVA-SAVI compositing method selects the observation closest to the nadir view since VA-SAVI values are reduced according to the sensor zenith angles. The higher sensor zenith angles, the smaller VA-SAVI values.

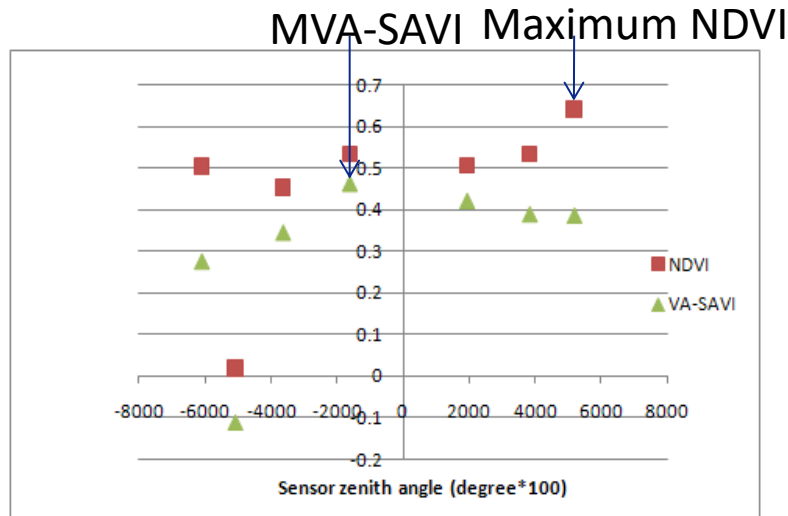


Figure 11. Comparison of the maximum value compositing and the maximum view angle adjusted SAVI compositing.

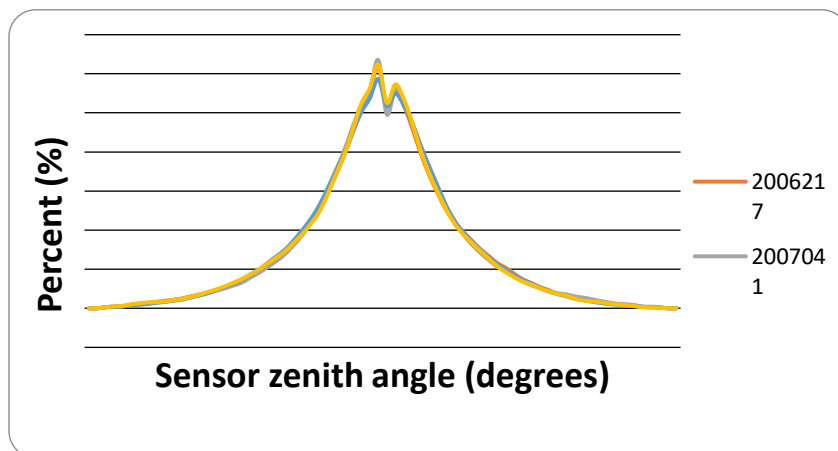


Figure 12. Histograms of sensor zenith angles composited by the MVA-SAVI method at different seasons.

The peaks of the histograms of sensor zenith angles composited by the MVA-SAVI method are close to the nadir at different seasons, indicating that observations close to the nadir view are more likely to be selected than the off-nadir observations (Figure 12).

The results of the compositing of eight daily VI values and the associated reflectances, QA flags, and solar/ view angles are written out in netCDF format in blocks that will be the input to further compositing to generate 16 day VIs. The eight day data blocks are also geographically mosaicked to produce the full global and regional data sets that are written out in netCDF format as the weekly VI EDRs. For each 16 day period, two sets of blocks of data from the first and second eight days of that 16 day period are composited to generate 16 day composite block data. The 16 day composite block data are geographically mosaicked and written out in netCDF format to generate the global and regional biweekly VI EDRs.

3.3.5 VI QA assignment

The daily gridded TOA and TOC reflectances and the derived VI products are subject to impact of environmental factors including cloud, aerosol and sun glint. Hence the quality assurances of derived VI products on the aggregated pixels are based on the cloud mask, quality flags in VIIRS Surface Reflectance data files, Aerosol Optical Thickness data files at granule level and the spatial aggregation scheme. The following section 3.3.5.1 describes the QA flag spatial aggregation scheme for NDE VIIRS VI products. Section 3.3.5.2 summarizes the VIIRS VI QFs in tables.

3.3.5.1. Spatial aggregation scheme for quality assurance of VIIRS VI products

The procedure for selecting pixels for aggregation and setting quality flags for the VI EDR output is shown as a flowchart in Figure 13. Only pixels taken from the same orbit will be considered for aggregation. A summary of the procedure follows:

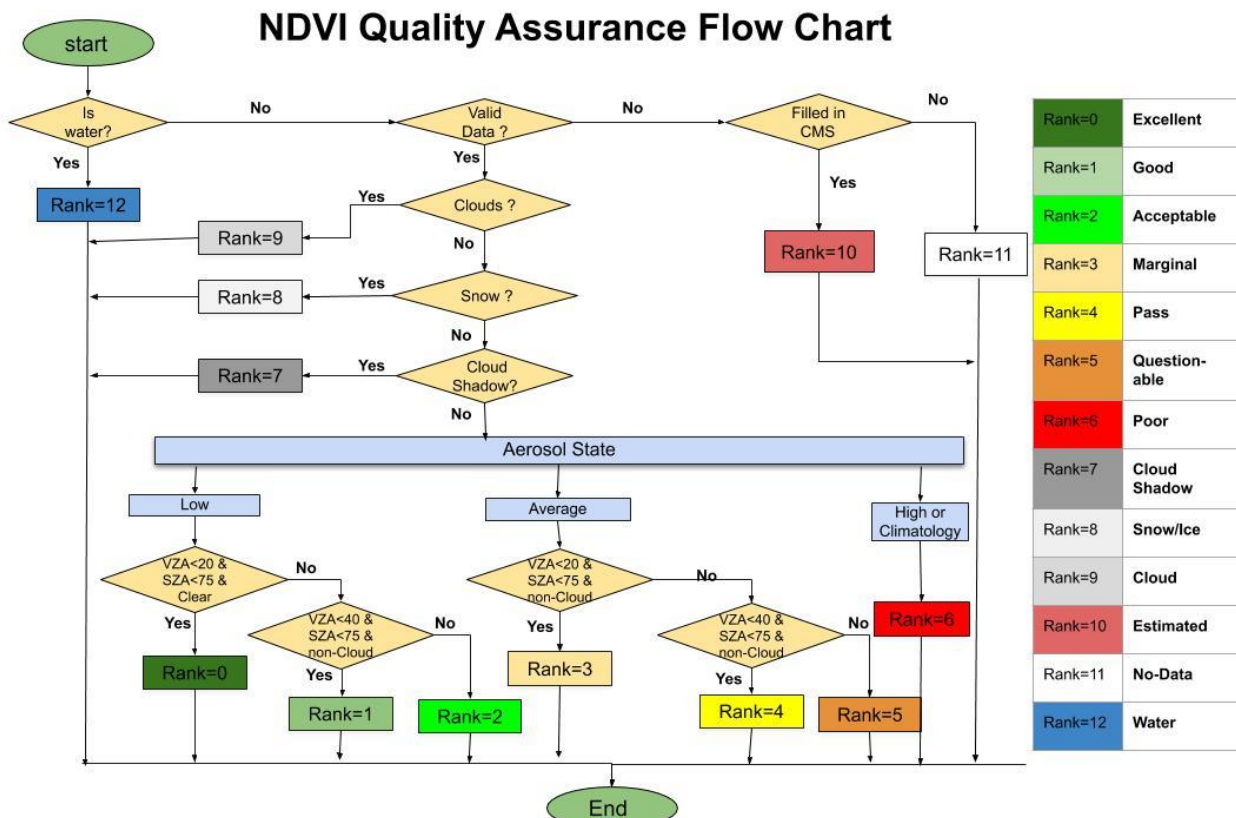


Figure 13: Flowchart for determining overall quality flag in an output VI grid cell

Step 1: If all available pixels in the grid area are water, set the overall quality flag value to 12, indicating a water pixel. Output VI values will be fill values.

Step 2: If no valid data are available, set the overall quality flag value to 10 if a fill value from climatology is used, or 11 if it is not.

Step 3: Reflectance values and cloud flag:

Check if the number of pixels with “confidently clear” is greater than or close to 80% of pixels (i.e., $n \geq 7$ for aggregating into 0.009° -grid, and $n \geq 115$ for aggregating into 0.036° -grid for the case where all fine grid cells are land covered and available from the same orbit). If this condition is met, average only those “confidently clear” pixels and set cloud flag on the

aggregated pixel as “confidently clear”. Other conditions will be checked (as described below) to evaluate an overall quality flag that will have a value between 0 and 8.

If the above condition is not met, check if the number of pixels with “confidently clear or probably clear” is greater than or close to 80% of pixels (i.e., $n \geq 7$ for aggregating into 0.009°-grid, and $n \geq 115$ for aggregating into 0.036°-grid in the case where all fine grid cells are land covered and available from the same orbit.). If this condition is met, average only those “confidently clear or probably clear” pixels and set cloud flag on the aggregated pixel as “probably clear”. Other conditions will be checked (as described below) to evaluate an overall quality flag that will have a value between 1 and 8.

If the two conditions above are not met, check if the number of pixels with “confidently clear or probably clear or probably cloudy” is greater than or close to 80% of pixels (i.e., $n \geq 7$ for aggregating into 0.009°-grid, and $n \geq 115$ for aggregating into 0.036°-grid for the case where all aggregated pixels are land and available from the same orbit). If this condition is met, then average only those “confidently clear or probably clear or probably cloudy” pixels and set cloud flag on the aggregated pixel as “probably cloudy”. Other conditions will be checked (as described below) to evaluate an overall quality flag that will have a value between 7 and 9. Otherwise, average all pixels and set cloud flag on the aggregated pixel as “confidently cloudy” and the overall quality flag value to 9.

Step 4: If a majority of the input pixels are snow covered, set the overall quality flag to 8. If any of the input pixels contain cloud shadow, set the overall quality to 7.

Step 5: If a majority of the pixels are low aerosol quantity, set overall quality flag value between 0 and 2 after obtaining sun/ view angle. If a majority of the pixels are average aerosol quantity, set overall quality flag value between 3 and 5 after obtaining sun/ view angle. If a majority of the pixels are high or climatology aerosol quantity, set overall quality flag value to 6. The criteria for making the further quality flag discriminations in this step are sun zenith angle, view zenith angle, and cloud flag as shown in Figure 13.

Step 6: Sun/View angle:

The three angular variables included in the VI EDR output are (i) sun zenith angle, (ii) view zenith angle, and (iii) relative azimuth angle. For each of these angles, angle values of pixels used for averaging in step 1 will be averaged to represent the angle value for the aggregated pixel. Only pixels within the same orbit are included when averaging sun/ view angles.

Step 7: Land/Water mask

The land/ water mask value for non-water aggregated grid cells will be the land surface type with the greatest number of pixels used in aggregation. If there are any land, desert, or snow pixels used in the aggregation, the pixel will have a land, desert, or snow type. If there are any land, desert, or snow pixels used in the aggregation, the surface type of the aggregation will be the surface type of the majority of the pixels with a land, desert, or snow surface type. If there is a tie between different surface types, the lower quality type will be selected. For land surface type, the rank order from high to low quality is land (not desert or snow), desert, and snow/ ice. The lower quality category will be selected in case of a tie.

Step 8: Values for other QFs for aggregated pixels will be determined by either “majority” or “worst case scenario”:

Aerosol Quantity: Use the majority value among pixels used for averaging in step 3. If there is a tie between different aerosol quantities, select the one of lower quality. The quality rank for aerosol categories from high to low is low aerosol, average aerosol, high aerosol, then climatology aerosol.

Cloud Shadow: set to “1” if any one pixel used for averaging in Step 3 has “Cloud Shadow = 1”.

3.3.5.2. QFs of VIIRS VI products

There are two QFs in the NVPS VI output files, listed as QF1 and QF2. These fields are bit-mapped quality fields for the inputs and outputs of the algorithm. They are listed in Table 6.

Table 6. Bit Layout of the Two QFs in the NVPS VI Product

Byte	VIIRS VI Flag	Result		Bits
QF1	Overall TOA NDVI Quality	0000 = Excellent 0001 = Good 0010 = Acceptable 0011 = Marginal 0100 = Pass 0101 = Questionable 0110 = Poor 0111 = Cloud Shadow	1000 = Snow/Ice 1001 = Cloud 1010 = Estimated (CMG) 1011 = No Data 1111 = Water/Ocean	4(bits 0-3)
(Refer to Figure 13 for a flowchart of how these values are determined.)				

NOAA NESDIS STAR

ALGORITHM THEORETICAL BASIS DOCUMENT

Version: 2.1

Date: May 18, 2021

TITLE: VIIRS VI Algorithm Theoretical Basis Document

Page 47 of 82

	Overall TOC NDVI Quality	0000 = Excellent 1000 = Snow/Ice 0001 = Good 1001 = Cloud 0010 = Acceptable 1010 = Estimated (CMG) 0011 = Marginal 1011 = NO Data 0100 = Pass 1111 = Water/Ocean 0101 = Questionable 0110 = Poor 0111 = Cloud Shadow (Refer to Figure 13 for a flowchart of how these values are determined.)	4 (bits 4-7)
QF2	EVI or EVI2	0 = EVI 1 = EVI2	1 (bit 0)
	Land Cover Type	00 = Snow/Ice 01 = Land 10 = Water/Ocean 11 = Desert	2 (bits 1-2)
	Cloud Confidence	00 = Confidently Clear 01 = Probably Clear 10 = Probably Cloudy 11 = Confidently Cloudy	2 (bits 3-4)
	Aerosol Quantity	00 = Climatology 01 = Low 10 = Average 11 = High	2 (bits 5-6)
	Cloud Shadow	0 = No Shadow 1 = Shadow	1 (bit 7)

3.4 Algorithm Output

The outputs of VIIRS VI system consist of three VI products, (TOA NDVI, TOC NDVI and TOC EVI) at three composite periods (daily, daily rolling 8-day, and daily rolling 16-day) at

two spatial resolutions (4-km global map and 1-km regional map). The three VI products are contained in the same VI EDR output files. Each compositing period and spatial resolution combination is represented by a separate EDR output file. For each composite period, the VIIRS VI system outputs include:

- (1) 4-km global TOA NDVI, TOC NDVI, TOC EVI, TOA I1 (red) reflectance, TOA I2 (NIR) reflectance, TOC I1 reflectance, TOC I2 reflectance, TOC M3 (blue) reflectance, QF1, QF2, solar zenith angle, view zenith angle and relative azimuth angle on a global geographic projection grid stored in a NetCDF file.
- (2) 1-km regional TOA NDVI, TOC NDVI, TOC EVI, TOA I1 (red) reflectance, TOA I2 (NIR) reflectance, TOC I1 reflectance, TOC I2 reflectance, TOC M3 (blue) reflectance, QF1, QF2, Solar zenith angle, view zenith angle and relative azimuth angle on a geographic projection grid stored in a NetCDF file.
- (3) Color-coded browse images of the global and regional TOA NDVI, TOC NDVI, TOC EVI maps, stored in six Geo-TIFF files.
- (4) Metadata: VI statistical data (maximum, minimum, mean and standard deviation over selected areas), which are useful for OSPO to monitor the VI product data quality and processing status, are saved in text files.

Table 7 lists all VIIRS VI output files and their characteristics.

Table 7. VIIRS VI Output Files

File	Description	Format	Size/file
VI-[DLY,WKL,BWKL]-REG _vxry_[npp,j01]_s[YYYYMMDD1]_e[YYYYMMDD1,8 or 16]_c[YYYYMMDDhhmmsss].nc	This is the daily, weekly or biweekly regional VI product	netCDF4	Typical file size 1.3 GB.
VI-[DLY,WKL,BWKL]-GLB _vxry_[npp,j01]_s[YYYYMMDD1]_e[YYYYMMDD1,8 OR 16]_c[YYYYMMDDhhmmsss].nc	This is the daily, weekly or biweekly global VI product	netCDF4	Typical file size 175 MB.
VI-TOA-NDVI-[DLY,WKL,BWKL]-REG _vxry_[npp,j01]_s[YYYYMMDD1]_e[YYYYMMDD1, OR 16]_c[YYYYMMDDhhmmsss].tif	Browse image of the TOA NDVI regional VI product	Geotiff	Typical file size 35 MB
VI-TOA-NDVI-[DLY,WKL,BWKL]-GLB _vxry_[npp,j01]_s[YYYYMMDD1]_e[YYYYMMDD1,8 OR 16]_c[YYYYMMDDhhmmsss].tif	Browse image of the TOA NDVI daily, weekly or biweekly global VI product	Geotiff	Typical file size 6 MB
VI-TOC-NDVI-[DLY,WKL,BWKL]-REG _vxry_[npp,j01]_s[YYYYMMDD1]_e[YYYYMMDD1,8 OR 16]_c[YYYYMMDDhhmmsss].tif	Browse image of the TOC NDVI daily, weekly or biweekly regional VI product	Geotiff	Typical file size 35 MB
VI-TOC-NDVI-[DLY,WKL,BWKL]-GLB _vxry_[npp,j01]_s[YYYYMMDD1]_e[YYYYMMDD1,8	Browse image of the TOC NDVI daily, weekly or	Geotiff	Typical file size 6 MB

NOAA NESDIS STAR

ALGORITHM THEORETICAL BASIS DOCUMENT

Version: 2.1

Date: May 18, 2021

TITLE: VIIRS VI Algorithm Theoretical Basis Document

Page 49 of 82

OR 16]_c[YYYYMMDDhhmmss].tif	biweekly global VI product		
VI-TOC-EVI-[DLY,WKL,BWKL]-REG _vxry_[npp,j01]_s[YYYYMMDD1]_e[YYYYMMDD1,8 OR 16]_c[YYYYMMDDhhmmss].tif	Browse image of the TOC EVI daily, weekly or biweekly regional VI product	Geotiff	Typical file size 35 MB
VI-TOC-EVI-[DLY,WKL,BWKL]-GLB _vxry_[npp,j01]_s[YYYYMMDD1]_e[YYYYMMDD1,8 OR 16]_c[YYYYMMDDhhmmss].tif	Browse image of the TOC EVI daily, weekly or biweekly global VI product	Geotiff	Typical file size 6 MB
VI-[DLY,WKL,BWKL]-REG _vxry_[npp,j01]_s[YYYYMMDD1]_e[YYYYMMDD1,8 OR 16]_c[YYYYMMDDhhmmss]_stat.txt	Statistics file of the daily, weekly or biweekly regional VI product for monitoring purposes	text	Typical file size 2 KB
VI-[DLY,WKL,BWKL]-GLB _vxry_[npp,j01]_s[YYYYMMDD1]_e[YYYYMMDD1,8 or 16]_c[YYYYMMDDhhmmss]_stat.txt	Statistics file of the daily, weekly or biweekly global VI product for monitoring purposes	text	Typical file size 2 KB

Table 8 lists VIIRS VI output file standard name description.

Table 8. VIIRS VI Output Files Standard Name Description

Sequence	Description
VI	Vegetation Indices (NDVI, EVI)
NDVI	Normal Difference Vegetation Index
EVI	Enhanced Vegetation Index
DLY	Daily (1-day temporal scale)
WKL	Weekly (8-day temporal resolution)
BWKL	Biweekly (16-day temporal resolution, in term of conventions)
GLB	Global (spatial resolution: 4-km)
REG	Regional (spatial resolution:1-km)
TOA	Top of Atmosphere
TOC	Top of Canopy
vxry	Version (e.g., v1r0)
npp	Indicates the observations are from S-NPP
j01	Indicates the observations are from NOAA20
s	start (data observation time)
e	end (data observation time)
c	current (data processing time)
YYYYMMDD	4-digit year, 2-digit month, and 2-digit day
hhmmss	2-digit hour, 2-digit minute, 2-digit second, and 1-digit fractional second

NOAA NESDIS STAR

ALGORITHM THEORETICAL BASIS DOCUMENT

Version: 2.1

Date: May 18, 2021

TITLE: VIIRS VI Algorithm Theoretical Basis Document

Page 50 of 82

.nc	netCDF4 file
.tif	GeoTiff image file
stat.txt	Text file stored statistics analysis results

The data structure of the VIIRS VI product includes the following data fields:

- 1) Three VI Products: NDVI_TOA, EVI_TOC and NDVI_TOC;
- 2) Five reflectance bands: I1_TOA, I2_TOA, I1_TOC, I2_TOC, and M3_TOC
- 3) Geometry Information: RAA: Relative Azimuth Angle, SZA: Solar Zenith Angle, and VZA: Viewing Zenith Angle;
- 4) Two Quality Flags (QFs).
- 5) Geospatial Coordinates: latitude, longitude

The description of the data fields in each VIIRS VI EDR output file is given in Table 9. The details of the bit layout of the two quality flags are listed in Table 6 in Section 3.3.5.

Table 9. Data Fields of the NVPS VI Product

Date Name	Data Description	Data Type	Dimension	Fill value	Scale	Offset	Data Range
NDVI_TOA	Top of Atmosphere Normalized Difference Vegetation Index	16-bit Integer	5000x10000 (Global) 10384x28889 (Regional)	-32768	10000	0	[-1, 1]
NDVI_TOC	Top of Canopy Normalized Difference Vegetation Index	16-bit Integer	5000x10000 (Global) 10384x28889 (Regional)	-32768	10000	0	[-1, 1]
EVI_TOC	Top of Canopy Enhanced Vegetation Index	16-bit Integer	5000x10000 (Global) 10384x28889 (Regional)	-32768	10000	0	[-1, 1]
I1_TOA	Top of Atmosphere Reflectance band	16-bit Integer	5000x10000 (Global) 10384x28889 (Regional)	-32768	10000	0	[0, 1]
I2_TOA	Top of Atmosphere Reflectance band	16-bit Integer	5000x10000 (Global) 10384x28889 (Regional)	-32768	10000	0	[0, 1]

NOAA NESDIS STAR

ALGORITHM THEORETICAL BASIS DOCUMENT

Version: 2.1

Date: May 18, 2021

TITLE: VIIRS VI Algorithm Theoretical Basis Document

Page 51 of 82

I1_TOC	Top of Canopy Reflectance band	16-bit Integer	5000x10000 (Global) 10384x28889 (Regional)	-32768	10000	0	[0, 1]
I2_TOC	Top of Canopy Reflectance band	16-bit Integer	5000x10000 (Global) 10384x28889 (Regional)	-32768	10000	0	[0, 1]
M3_TOC	Top of Canopy Reflectance band	16-bit Integer	5000x10000 (Global) 10384x28889 (Regional)	-32768	10000	0	[0, 1]
SZA	Solar Zenith Angle	16-bit Integer	5000x10000 (Global) 10384x28889 (Regional)	-32768	100	0	[0,90]
VZA	Viewing Zenith Angle	16-bit Integer	5000x10000 (Global) 10384x28889 (Regional)	-32768	100	0	[0,90]
RAA	Relative Azimuth Angle	16-bit Integer	5000x10000 (Global) 10384x28889 (Regional)	-32768	100	0	[-180,180]
QF1	Quality Flag Byte 0 (See Table 3-5)	8-bit unsigned character	5000x10000 (Global) 10384x28889 (Regional)	255	1	0	[0, 255]
QF2	Quality Flag Byte 1 (See Table 3-5)	8-bit unsigned character	5000x10000 (Global) 10384x28889 (Regional)	255	1	0	[0, 255]
Latitude	Geospatial coordinate	32-bit float	5000x1 (Global) 10384x1 (Regional)	-999.0	1	0	[-90,90] [-7.5,90]
Longitude	Geospatial coordinate	32-bit float	10000x1 (Global) 28889x1 (Regional)	-999.0	1	0	[-180,180] 130E->30E

An example of the overall metadata information of the NVPS VI Product is shown in Table 10.

Table 10. Metadata Information Example for the NVPS VI Product

<p>Number of attributes = 29</p> <p>Conventions = CF-1.5 Metadata_Conventions = CF-1.5, Unidata Dataset Discovery v1.0 cdm_data_type = grid creator_email = yunyue.yu@noaa.gov/marco.vargas@noaa.gov creator_name = DOC/NOAA/NESDIS/STAR > VI Team, Center for Satellite Applications and Research, NESDIS, NOAA, U.S. Department of Commerce creator_url = https://www.star.nesdis.noaa.gov/smcd/viirs_vi/Monitor.htm date_created = 2017-11-03T19:23:18Z geospatial_bounds = POLYGON((-180.0 90.0, 180.0 90.0, 180.0 -90.0, -180.0 -90.0, -180.0 90.0)) geospatial_lat_resolution = 0.036 geospatial_lat_units = degrees_north geospatial_lon_resolution = 0.036 geospatial_lon_units = degrees_east history = Created by VI algorithm v1.0 id = 51bfbb25-4be3-42cf-8932-68b26acfd5f institution = DOC/NOAA/NESDIS/NDE > S-NPP Data Exploitation, NESDIS, NOAA, U.S. Department of Commerce instrument_name = VIIRS naming_authority = gov.noaa.nesdis.nde platform_name = NPP [or NOAA20] process_level = NOAA Level 3 project = S-NPP Data Exploitation publisher_email = espcoperations@noaa.gov publisher_name = DOC/NOAA/NESDIS/NDE > S-NPP Data Exploitation, NESDIS, NOAA, U.S. Department of Commerce publisher_url = http://projects.osd.noaa.gov/NDE source = GITCO, JRR-AOD, JRR-CloudMask, SR, SVI01, SVI02 standard_name_vocabulary = CF Standard Name Table (version 17, 24 March 2011) summary = TOA NDVI, TOC NDVI and TOC EVI in each pixel derived on a daily basis from VIIRS observations time_coverage_end = 2017-10-20T24:00:00Z time_coverage_start = 2017-10-20T00:00:00Z title = VIIRS_VI</p>
<p>Conventions = CF-1.5 Metadata_Conventions = CF-1.5, Unidata Dataset Discovery v1.0 cdm_data_type = grid creator_email = yunyue.yu@noaa.gov/marco.vargas@noaa.gov</p>

```
creator_name = DOC/NOAA/NESDIS/STAR > VI Team, Center for Satellite
Applications and Research, NESDIS, NOAA, U.S. Department of Commerce
creator_url = https://www.star.nesdis.noaa.gov/smcd/viirs_vi/Monitor.htm
date_created = 2017-11-03T20:19:53Z
geospatial_bounds = POLYGON((130.0 90.0, 30.0 90.0, 30.0 -7.5, 130.0 -7.5, 130.0
90.0))
geospatial_lat_resolution = 0.0090
geospatial_lat_units = degrees_north
geospatial_lon_resolution = 0.0090
geospatial_lon_units = degrees_east
history = Created by VI algorithm v1.0
id = a43c72a3-1f14-4edf-8dbe-06b97a7bcb49
institution = DOC/NOAA/NESDIS/NDE > S-NPP Data Exploitation, NESDIS, NOAA,
U.S. Department of Commerce
instrument_name = VIIRS
naming_authority = gov.noaa.nesdis.nde
platform_name = NPP [or NOAA20]
process_level = NOAA Level 3
project = S-NPP Data Exploitation
publisher_email = espcoperations@noaa.gov
publisher_name = DOC/NOAA/NESDIS/NDE > S-NPP Data Exploitation, NESDIS,
NOAA, U.S. Department of Commerce
publisher_url = http://projects.osd.noaa.gov/NDE
source = GITCO, JRR-AOD, JRR-CloudMask, SR, SVI01, SVI02
standard_name_vocabulary = CF Standard Name Table (version 17, 24 March 2011)
summary = TOA NDVI, TOC NDVI and TOC EVI in each pixel derived on a daily
basis from VIIRS observations
time_coverage_end = 2017-10-20T24:00:00Z
time_coverage_start = 2017-10-20T00:00:00Z
title = VIIRS_VI
```

3.5 *Practical Considerations*

3.5.1 Numerical computation consideration

The whole algorithm is composed of many straight forward calculations, thus, it is light computationally.

3.5.2 Programming and procedural consideration

The VIIRS VI code runs every day with all the available SNPP input data for making the daily composites. Daily rolling 8-day composites are produced from the daily composites. Daily rolling 16-day composites are produced from the 8-day composites. Global and regional VI products are both produced on a daily, daily rolling 8-day, and daily rolling 16-day basis. The compositing is performed in blocks in order to perform computations in parallel and speed up processing.

3.5.3 Quality assessment and diagnostics

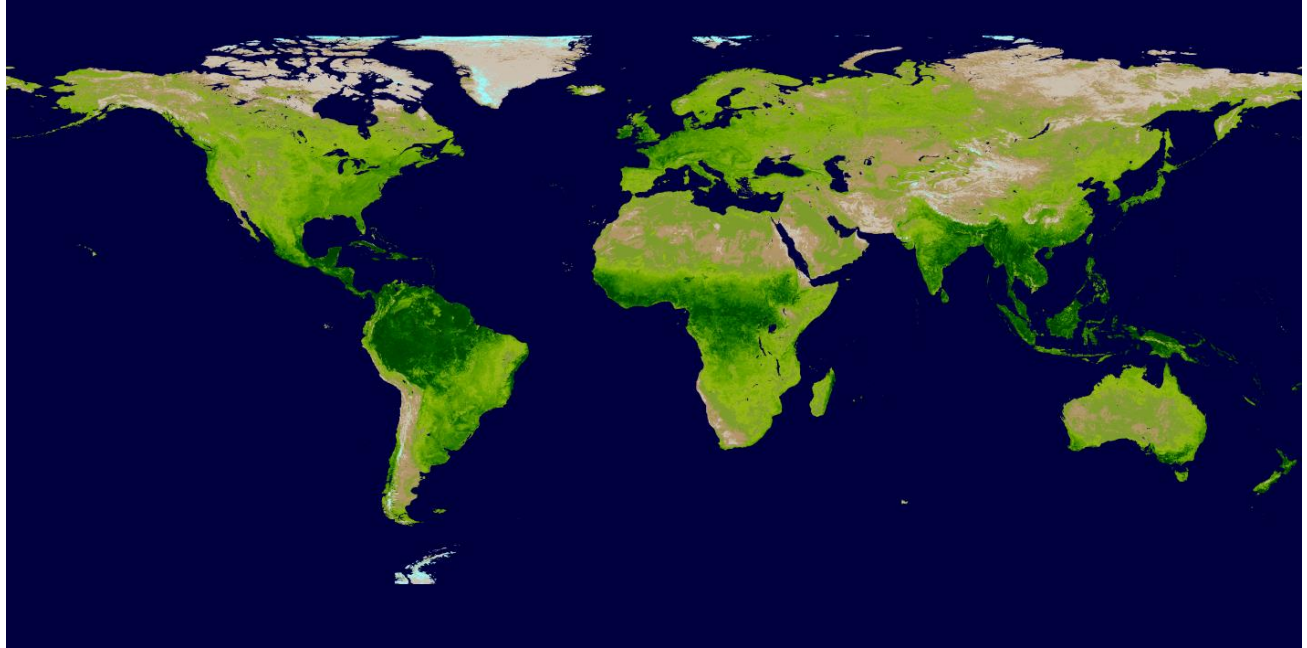
Unit testing and system testing include quality assessment of the VI products. Section 3.7 describes the validation of the VIIRS VI product with the MODIS VI products, validation through comparison of NPP to NOAA20 VIIRS VI products, and evaluation against PhenoCam in situ data.

3.5.4 Exception handling

The expected exceptions, and a description of how they are identified, trapped, and handled, are provided in the system maintenance manual.

3.6 *Sample Results*

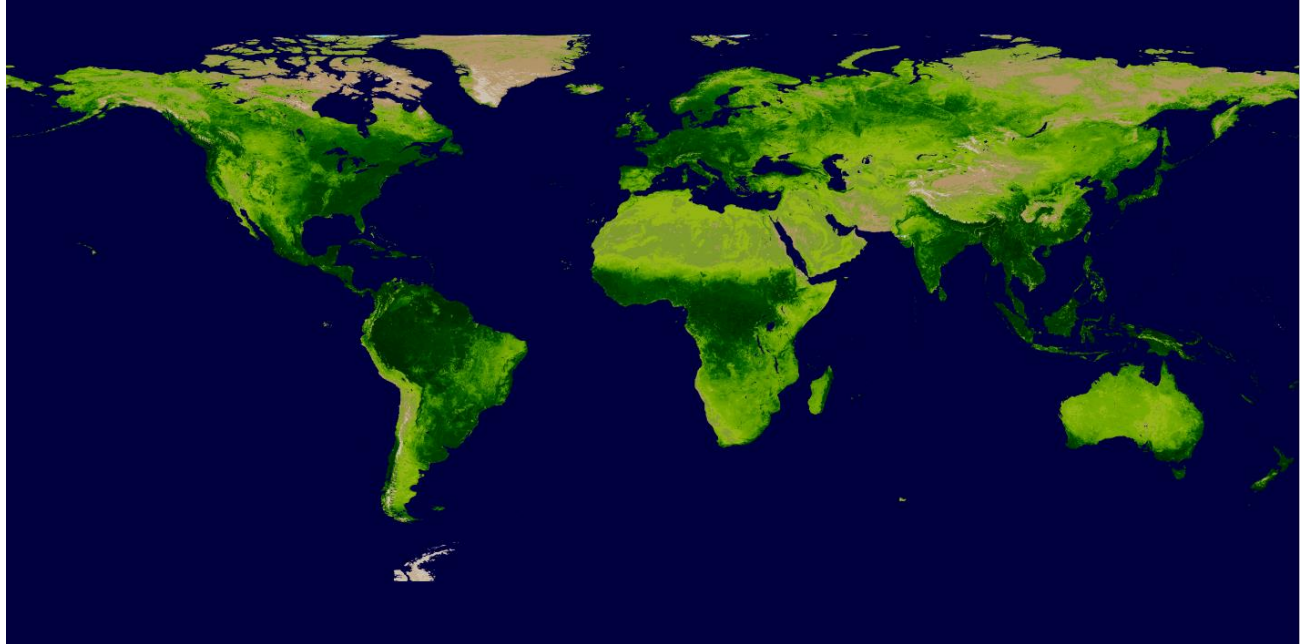
For visual examination of product quality, color-coded VI browse images in GeoTiff format for the global and regional VI products are shown in Fig. 10. The dimensions of the 0.036° resolution global VI browse image are 10000 and 5000. The dimensions of the 0.009° resolution regional VI browse image are 28889 and 10834.



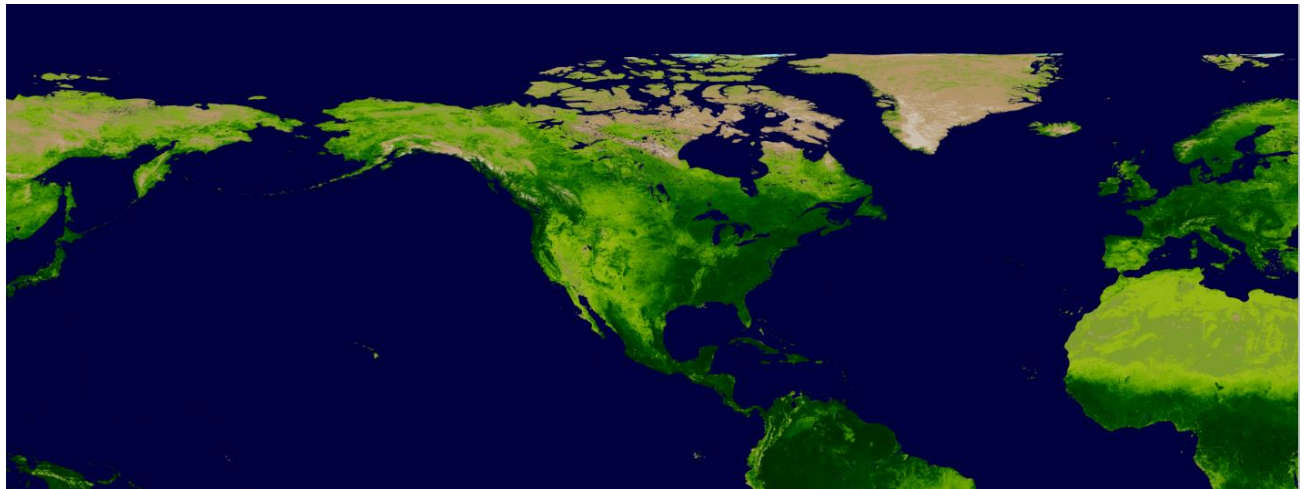
(a)



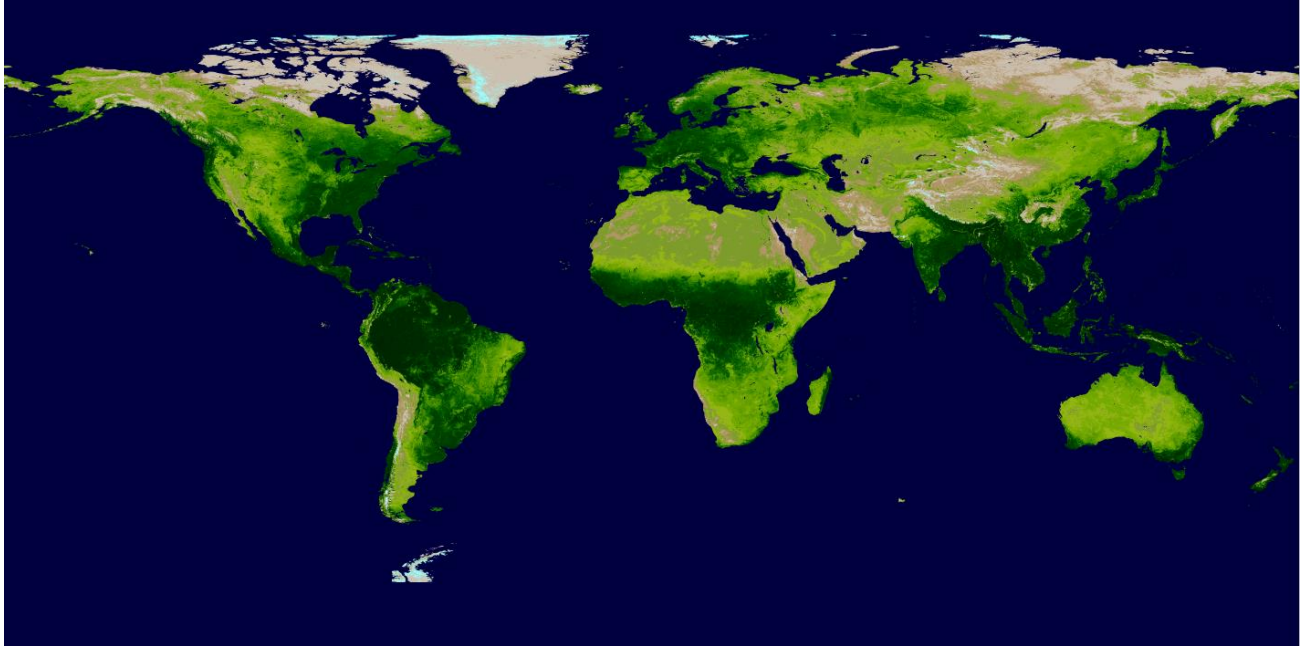
(b)



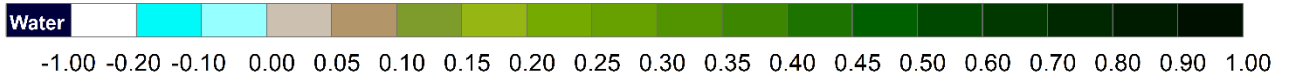
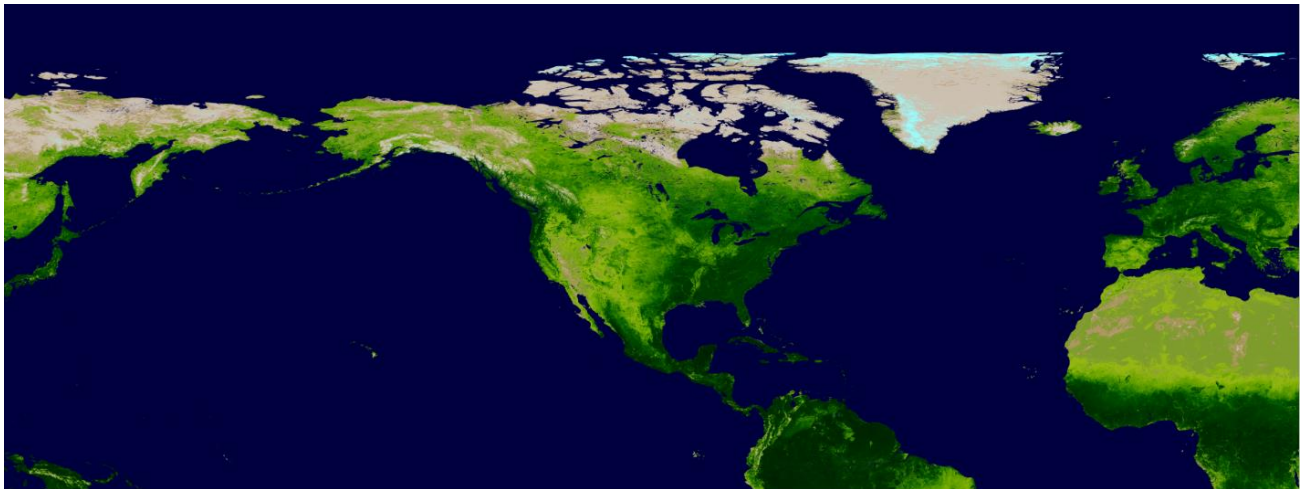
(c)



(d)



(e)



(f)

Figure 14. VIIRS VI browse images in the week of Oct 5-20, 2017. (a) VIIRS TOC global 0.036° 16-day composite EVI; (b) VIIRS TOC regional 0.009° 16-day composite EVI; (c) VIIRS TOA global 0.036° 16-day composite NDVI; (d) VIIRS TOA regional 0.009° 16-day composite NDVI; (e) VIIRS TOC global 0.036° 16-day composite NDVI; (f) VIIRS TOC regional 0.009° 16-day composite NDVI.

3.7 Validation Efforts

3.7.1 Validation strategy

The initial VIIRS VI product validation process started in 2013 when the S-NPP VIIRS reached the provisional maturity stage in the IDPS system (Vargas et al., 2013). Results of the IDPS VIIRS data validation can be inherited by this NDE VIIRS VI product since the product algorithms are basically the same. Additionally, the NDE VI products have been and will be evaluated and validated by

- ▶ Product inter-comparison with other satellites (e.g., MODIS, AVHRR, Landsat, etc.) over overlapping orbital tracks and over a globally-distributed set of sites;
- ▶ Time series comparison with in situ VI data and vegetation productivity (e.g., gross primary productivity) data over FLUXNET and PhenoCam sites;
- ▶ Cross-comparison with AERONET-processed data.

VIIRS VI measurement accuracy, precision and uncertainty are calculated according to Eqs. 3.7-3.10. Accuracy is defined as the magnitude of the mean measurement error,

$$accuracy = |\mu| \quad (3.7)$$

where μ is the mean measurement error.

$$\mu = \frac{\sum_{i=1}^n (VIIRS_VI_i - ref_VI_i)}{n} \quad (3.8)$$

where ref_VI is the reference VI to be compared with the VIIRS VI. Precision is defined as the standard deviation of the measurement errors.

$$Precision = \left[\frac{1}{n-1} \sum_{i=1}^n (VIIRS_VI_i - ref_VI_i - \mu)^2 \right]^{1/2} \quad (3.9)$$

Uncertainty is defined as the root mean square error (RMSE).

$$Uncertainty = \left[\frac{1}{n} \sum_{i=1}^n (VIIR_VI_i - ref_VI_i)^2 \right]^{1/2} \quad (3.10)$$

3.7.2 Validation of VIIRS VI EDR granule product

The early version of the VIIRS VI EDR data were generated daily at the imagery resolution (375m at nadir) over land in swath/granule format (JPSS VVI ATBD, 2011). The data product ID for the VI EDR is VIVIO (VIIRS vegetation index operational product). An initial assessment of the SNPP VIIRS VI EDR was conducted by Vargas, Miura, Shabanov and Kato (2013). In this assessment analysis, VIIRS, Aqua MODIS, and NOAA-18 AVHRR VI products over the period 2 May 2012 to 31 March 2013 were used. VIIRS Vegetation Index (VIVIO), Surface Reflectance (IVISR), and Geolocation (GIMGO) products in granule format were obtained and used to generate daily global gridded TOA NDVI and TOC EVI, and corresponding QF and geometry data sets. The MODIS data sources were Aqua MODIS 16-day TOC EVI (MYD13A2 Collection 5) in the gridded MODIS tile format (set of 1 km MODIS Land tiles, sinusoidal projection), Aqua MODIS daily TOA reflectance (MYD02HKM Collection 5) in the swath format, and daily TOC reflectances (MYD09CMG Collection 5) in the Climate Modeling Grid (CMG) format (geographic projection, 0.05 degree). The daily MODIS data were processed into daily TOA NDVI and TOC EVI. Two types of analyses focused on an assessment of physical (global scale) and radiometric (regional scale) performances of VIIRS VI EDR.

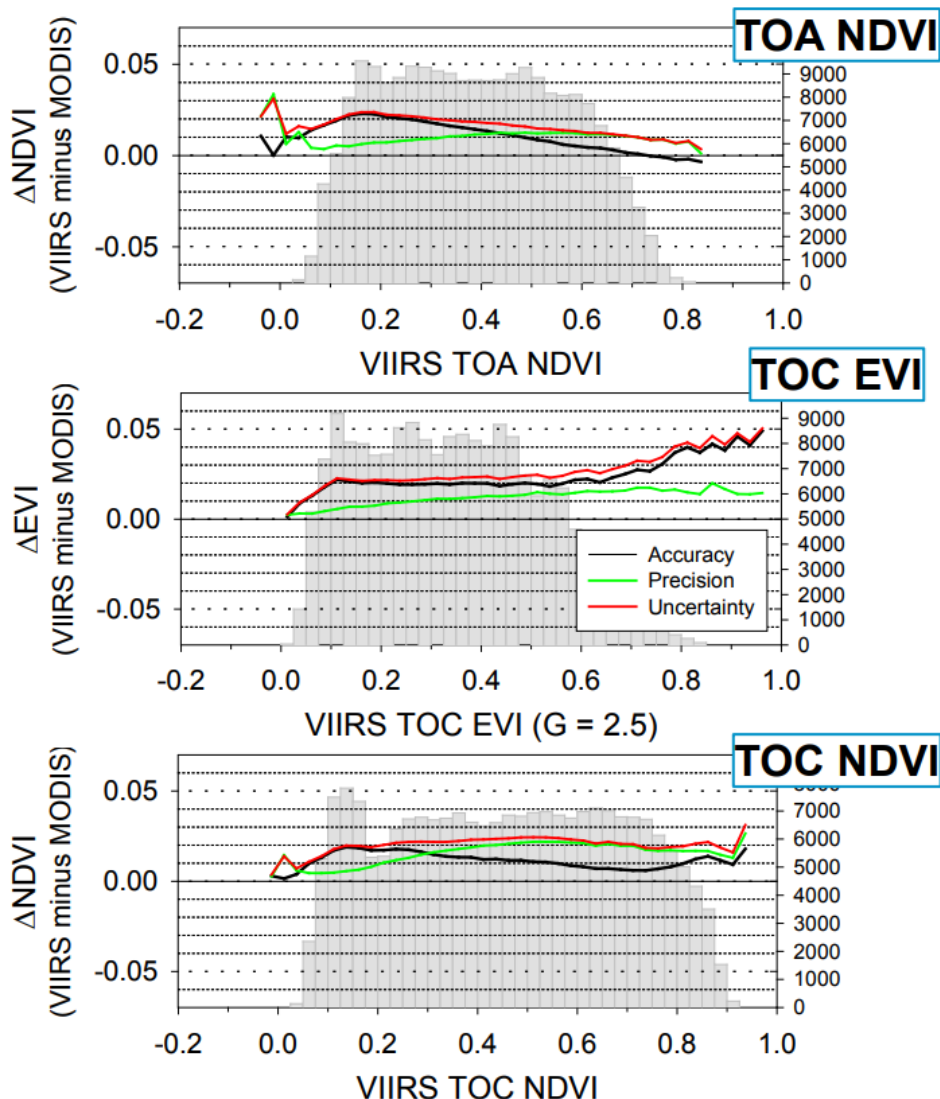


Figure 15. VIIRS TOA NDVI, TOC EVI and TOC NDVI Accuracy, Precision and Uncertainty (APU) are plotted as function of VIIRS VI values in global inter-comparison with MODIS VI.

The Accuracy, Precision and Uncertainty (APU) of VIIRS TOA NDVI, TOC NDVI and TOC EVI data were calculated using the counterpart VI calculated from the Aqua MODIS data as reference data. Fig.15 shows the APU of VIIRS VI as functions of VIIRS VI values. VIIRS TOA NDVI accuracy and uncertainty decreased with the increase of VI values, whereas the TOC EVI accuracy and uncertainty increased with the increase of VI values, particularly when EVI is larger than 0.7. TOC NDVI has relatively stable APU with the increase of VI values.

Fig. 12 shows the APU time series of the VIIRS TOA NDVI, TOC NDVI and TOC EVI in global inter-comparison with the MODIS VI. TOA NDVI APU were stable and less than 0.02 in the whole year. TOC NDVI APU showed slight seasonal variation. The uncertainty increased from DOY 250 to 280 and accuracy increased from DOY 180 to 280. TOC EVI accuracy and uncertainty also showed slightly seasonal variation with peaks at DOY 30 and DOY 180-220, whereas its precision is relatively stable in the whole year.

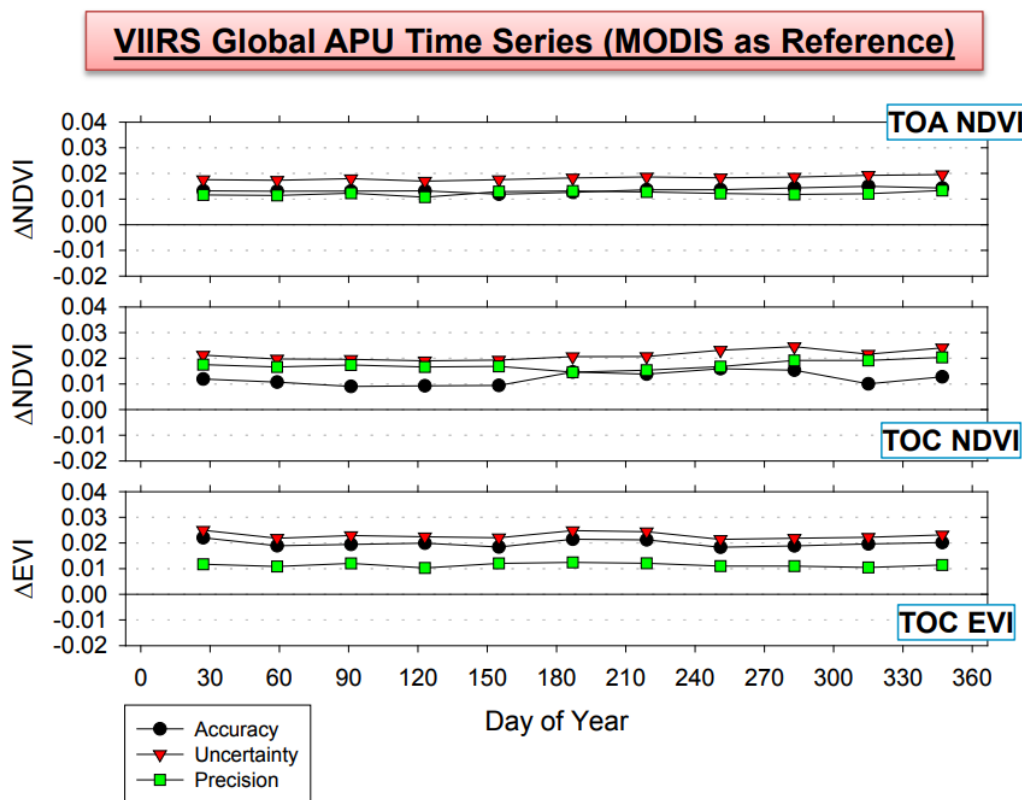


Figure 16. VIIRS TOA NDVI, TOC EVI and TOC NDVI Accuracy, Precision and Uncertainty (APU) time series in global inter-comparison with MODIS VI.

The VIIRS VI EDR global APU are summarized in Table 11 . TOA NDVI has relatively small APU values, with an accuracy 0.013 NDVI unit, precision 0.012 and uncertainty 0.018. The accuracy and uncertainty of TOC NDVI were higher than those of TOA NDVI. The precision of TOC EVI was higher than those of TOA and TOC NDVI. Overall the VIIRS VI EDR met

the Joint Polar Satellite System Program Level 1 Requirements Supplement (L1RDS) thresholds (Refer to Table 1 in this document and https://www.jpss.noaa.gov/assets/pdfs/technical_documents/L1RDS.pdf)

Table 11. VIIRS VI EDR global APU estimation

	TOA NDVI	TOC NDVI	TOC EVI	L1RDS threshold
Accuracy	0.013	0.020	0.012	0.05
Precision	0.012	0.011	0.018	0.04
Uncertainty	0.018	0.023	0.021	0.06

Miura, Muratsuchi and Vargas (2018) extended the assessment of the VIIRS VI EDR granule product (Vargas et al. 2013) and cross-compared SNPP VIIRS VI EDR and MODIS VIs using near-coincident observation pairs obtained across the globe for the year 2015. In this VIIRS VI vs. MODIS VI comparison study, VIIRS and MODIS products were obtained for 3 days every month for the year 2015 when MODIS and VIIRS orbit tracts overlapped. VIIRS VI EDR, daily TOA and surface reflectances, and geo-angle products were obtained from the Level-1 and Atmosphere Archive and Distribution System (LAADS) Distributed Active Archive Center (DAAC) (<https://ladsweb.modaps.eosdis.nasa.gov>). MODIS Collection 6 daily 500-m TOA and surface reflectance (MYD02HKM and MYD09, respectively), and geo-angle (MYD03) products were also obtained from the LAADS DAAC.

All of the unprojected VIIRS and MODIS granule data were first projected onto a geographic projection grid with nearest neighbor resampling and stitched into daily global mosaics. The grid sizes of 0.0036° by 0.004° and 0.004° by 0.004° were adopted for VIIRS and MODIS, respectively. Then the global mosaic data were spatially-aggregated into a coarser grid (0.036° by 0.040° or ~ 4 km), for meeting the JPSS VIIRS VI gridded product requirement. Miura, Muratsuchi and Vargas (2018) found that VIIRS VIs were slightly higher than the MODIS counterparts by 0.012-0.020 for the three VIs (see accuracy in Table 12). TOA NDVI and TOC NDVI cross-sensor differences were found to be not seasonally nor view zenith angle-dependent, whereas TOC EVI and TOC EVI2 cross-sensor differences were found to be view zenith angle dependent where systematic differences increased with increasing view zenith angles (Miura et al. 2018). By band decomposition analysis, Miura et al. (2018) also found that NIR reflectance difference dominates the VIIRS-MODIS cross-sensor TOA NDVI difference (which is small). The TOC EVI difference is dominated by the observed view zenith angle differences.

Using the MODIS VI product as reference, the APU values of the VIIRS VI EDR were calculated and listed in Table 12. The VIIRS TOA NDVI has relatively small uncertainty (0.018), and the TOC NDVI and EVI have a slightly higher uncertainty, 0.021 and 0.022, respectively. The VIIRS VI EDR met the Joint Polar Satellite System Program Level 1 Requirements Supplement (L1RDS) thresholds again in this assessment.

Table 12. VIIRS VI EDR global APU estimation in comparison with MODIS VIs

	TOA NDVI	TOC NDVI	TOC EVI	L1RDS threshold
Accuracy	0.013	0.012	0.020	0.05
Precision	0.012	0.017	0.011	0.04
Uncertainty	0.018	0.021	0.022	0.06

3.7.3 Validation of VIIRS gridded and composited VI products

Comprehensive validation of gridded VIIRS VI EDRs over global coverage and long time series comparison against the reference data (i.e., the *in situ* data and other satellite VI products) will be performed on an ongoing basis throughout the product calibration and validation phase. The NOAA20 VIIRS Vegetation Index EDR achieved validated maturity in April 2020. This section will summarize validation work that has been performed up to that point as well as describing plans for further validation.

3.7.3.1 Validation data

It is desirable to have a long time series of VIIRS VI EDR data for validation purposes. It is also desirable to have VI EDRs from multiple VIIRS instruments for purposes of cross-comparison. Validation has been performed with NPP VIIRS EDR data from March 2019 through January 2020, and NOAA20 VIIRS EDR data from June 2019 through January 2020. The time series length of VIIRS VI EDR data available for validation is expected to increase through ongoing data production and potentially through reprocessing in the future. With the launch of J02 VIIRS, VI EDR data from an additional VIIRS instrument should become available in future years.

NASA produces a global 8-day rolling biweekly (16-day) vegetation index product from NPP VIIRS data. This product includes TOC NDVI, TOC EVI, and TOC EVI2. A similar global 16-day vegetation index product including TOC NDVI and TOC EVI is produced by NASA from MODIS data. Both of these data sets are useful for comparison to the NOAA-produced VIIRS VI EDRs. Information about the global gridded NASA NPP VIIRS VI data product is available at <https://lpdaac.usgs.gov/products/vnp13c1v001/>, and information about the global gridded

NASA MODIS VI product is available at <https://lpdaac.usgs.gov/products/mod13c1v006/>. The NASA products are defined on a 0.05 degree grid. The discrepancy between this grid and the NOAA VI global grid is addressed by interpolating the NASA data to the NOAA grid through cubic convolution.

The primary source of in situ data used for validation of the VIIRS VI EDR so far is the PhenoCam network of phenology monitoring cameras (<https://phenocam.sr.unh.edu/webcam/>). The PhenoCam cameras cover a wide variety of climate and ecosystem types. PhenoCam cameras take multiple RGB images of the same field of view every day. These data are available as raw imagery or as daily or 3-day time series of green chromatic coordinate (GCC), defined as

$$GCC = DN_{Green} / (DN_{Blue} + DN_{Green} + DN_{Red}) \quad (3.11)$$

where DN_{Blue} , DN_{Green} , and DN_{Red} are the total digital number counts in the blue, green, and red components of an RGB image, respectively. A gray image (equal DN_{Blue} , DN_{Green} , and DN_{Red} components) has a GCC of 0.33. Varying degrees of greenness are typically characterized by GCC values ranging from 0.35 to 0.45.

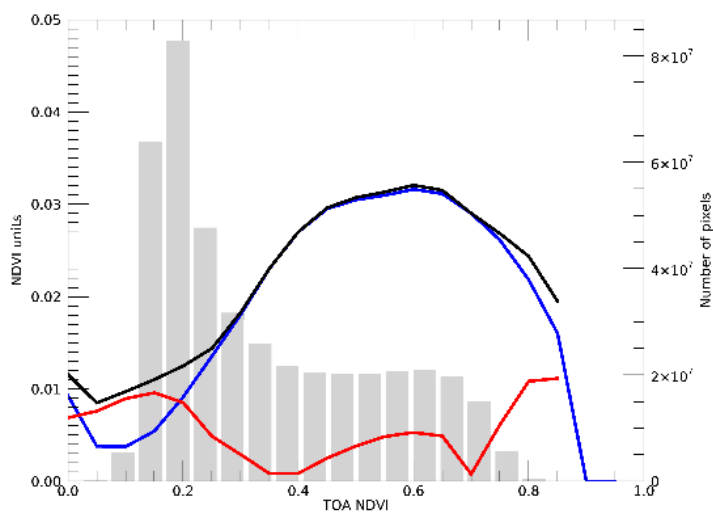
An additional source of in-situ data for comparison to VIIRS VI EDRs is the FLUXNET network of flux tower sites. Information about FLUXNET is available at https://daac.ornl.gov/cgi-bin/dataset_lister.pl?p=9. At some of the FLUXNET sites, incoming and outgoing shortwave and longwave radiation are measured, which allows for the generation of an in-situ vegetation index that is similar to, but not directly comparable to, vegetation indices as measured by satellites. Some FLUXNET sites also measure gross primary productivity (GPP), which can be expected to exhibit correlation with and similar temporal variations as satellite vegetation index.

3.7.3.2 Comparison Results

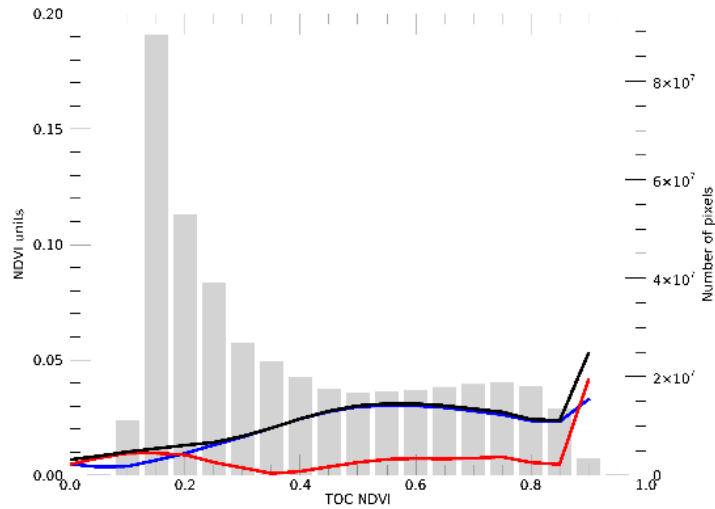
NPP and NOAA20 vegetation index comparisons are shown in Figure 17. The first three images show biweekly global NPP vs. NOAA20 differences stratified by NPP VI value for the period June 2019 through January 2020. Accuracy, precision, and uncertainty are shown in red, blue, and black lines respectively, and histograms of overall numbers of NPP VI pixels in different value ranges are shown in gray. The results for TOA NDVI are shown in (a), for TOC NDVI in (b), and TOC EVI in (c). The plots (d), (e), and (f) are time series of global accuracy, precision, and uncertainty for NPP vs. NOAA20 TOA NDVI, TOC NDVI, and TOC EVI, respectively. Table 13 shows the overall global biweekly NPP vs. NOAA20 accuracy,

precision, and uncertainty statistics. Figure 17 and Table 13 show that the accuracy and precision for all three vegetation indices are within the specification for the VIIRS VI EDR overall and throughout the time period considered. However, for high VI values, the accuracy, precision, and uncertainty are much higher than for low VI values. Since there are substantially fewer high VI pixels than low VI pixels, this has little effect on the overall evaluation of product quality. As more VI EDR processing is performed, additional high VI value data will be produced, enabling further investigation of the worse consistency between NPP and NOAA20 VIIRS VI values when those values are high. Similar analyses were also performed for regional VIs and for the daily and biweekly products, and produced similar results.

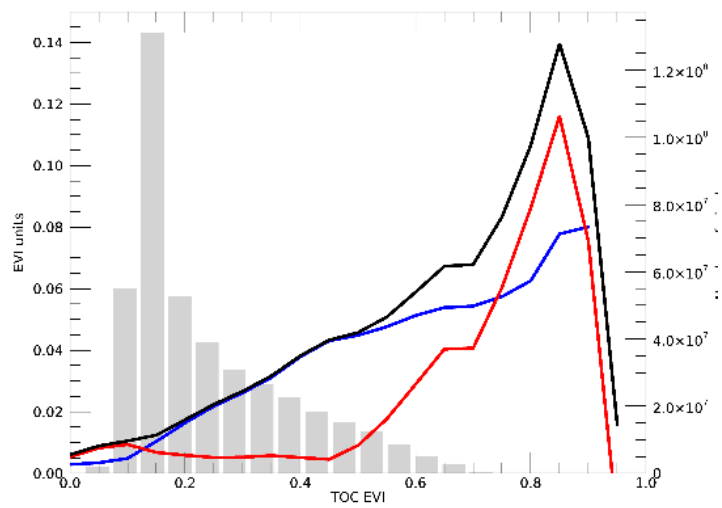
(a)



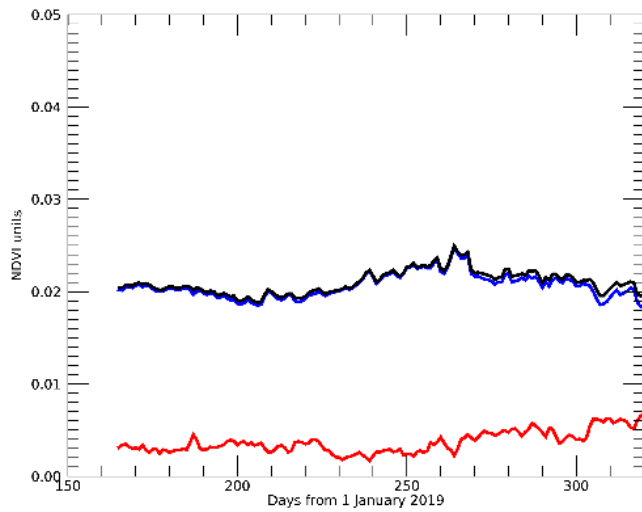
(b)



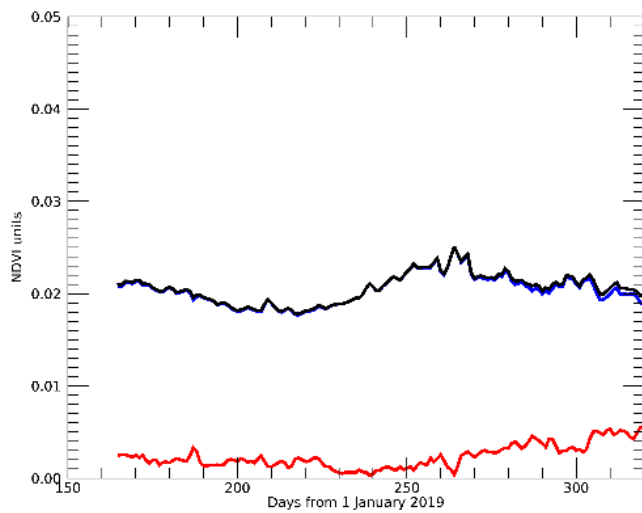
(c)



(d)



(e)



(f)

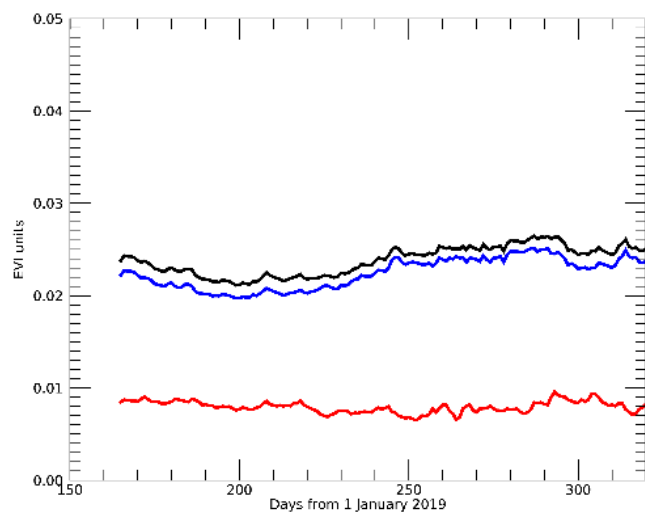


Figure 17: Accuracy (red), precision (blue), and uncertainty (black) statistics for biweekly global NPP vs. NOAA20 vegetation index. (a), (b), and (c) are stratified by NPP VI value, with histograms of total numbers of pixels in each value bin shown in gray. (a) TOA NDVI. (b) TOC NDVI. (c) TOC EVI. (d), (e), and (f) show time series statistics. (d) TOA NDVI. (e) TOC NDVI. (f) TOC EVI.

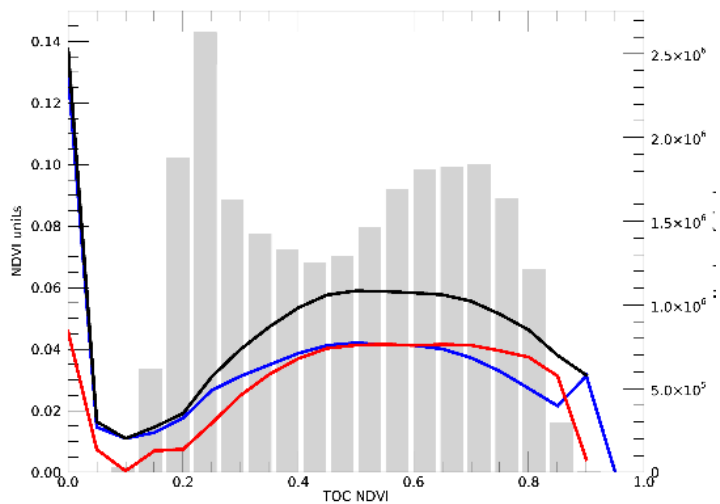
Table 13. Overall statistics for NPP vs. NOAA20 vegetation indices.

	TOA NDVI	TOC NDVI	TOC EVI
Accuracy	0.0039	0.0026	0.0080
Precision	0.2031	0.0202	0.0219
Uncertainty	0.0207	0.0203	0.0233

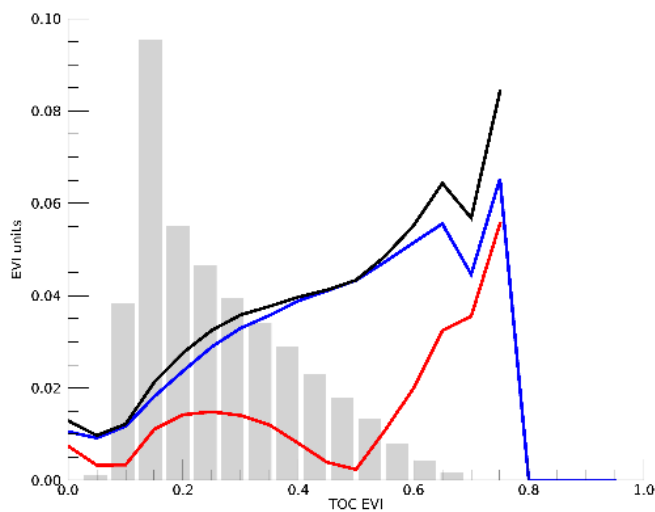
Statistical comparisons for biweekly NOAA vs. NASA NPP VIIRS TOC NDVI and TOC EVI for the period April 2019 through January 2020 are shown in Figure 18. Figure 18-(a) and Figure 18-(b) show the results when stratified by NOAA NPP VI value, similar to Figure 17-(a, b, c) above. Figure 18-(c) and Figure 18-(d) show time series statistics for this comparison. Table 14 shows the overall statistics for the NOAA vs. NASA NPP VIIRS VI comparisons. The results are similar to those found with NPP vs. NOAA20 comparisons, with accuracy and

precision statistics meeting the requirements overall and throughout the time period considered, but not for especially high values of vegetation index.

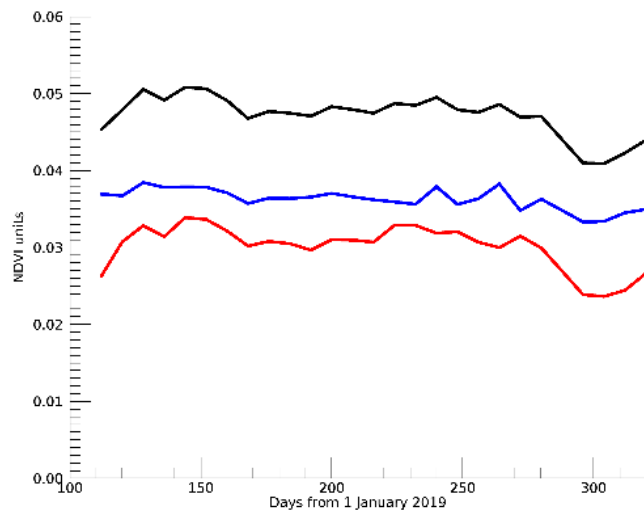
(a)



(b)



(c)



(d)

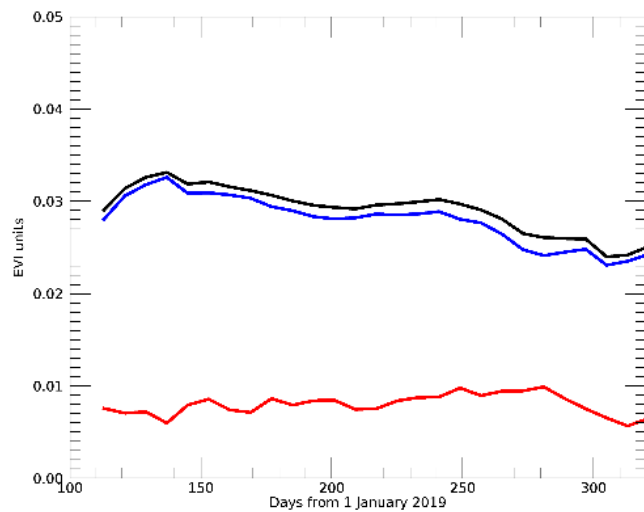


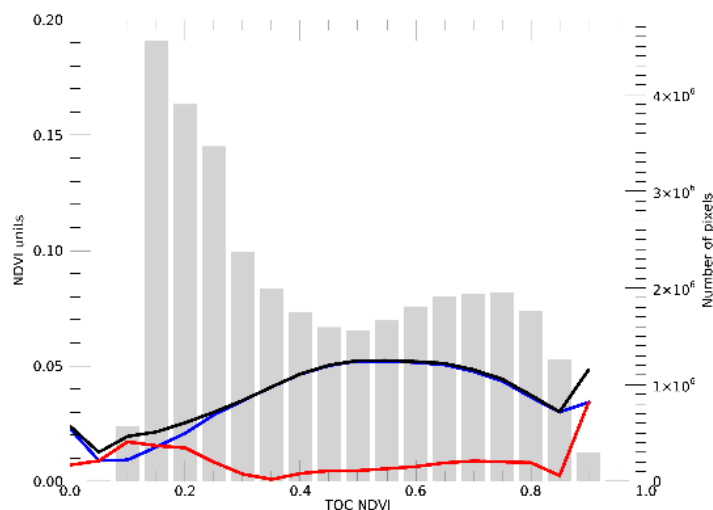
Figure 18: Accuracy (red), precision (blue), and uncertainty (black) statistics for NOAA vs. NASA NPP VIIRS vegetation indices. (a) and (b) are stratified by NOAA VI value, with histograms of numbers of pixels shown in gray. (a) TOC NDVI. (b) TOC EVI. Time series are shown in (c) and (d). (c) TOC NDVI. (d) TOC EVI.

Table 14. Overall statistics for comparison of NOAA to NASA NPP VIIRS VIs.

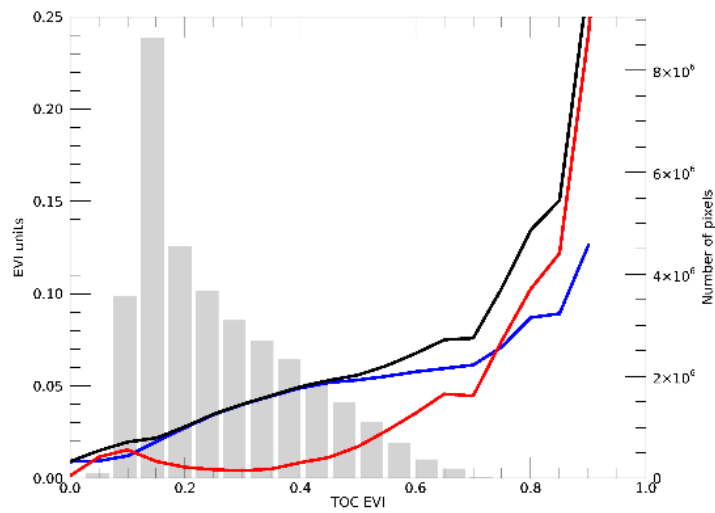
	TOC NDVI	TOC EVI
Accuracy	0.0298	0.0077
Precision	0.0361	0.0287
Uncertainty	0.0468	0.0276

Figure 19 shows the results of comparison between biweekly global NOAA NPP VIIRS and MODIS vegetation indices for the period June 2019 through January 2020, again with accuracy shown in red, precision in blue, and uncertainty in black. Figures 19-(a) and 19-(b) show the statistics stratified by NPP VIIRS VI value, with number of pixels by value shown as a histogram in gray. Figures 19-(c) and 19-(d) show time series statistics for this comparison. Table 15 shows the overall statistics for the biweekly global NPP VIIRS versus MODIS VIs. All the results are within the VIIRS product specifications, except for TOC EVI at high VI values.

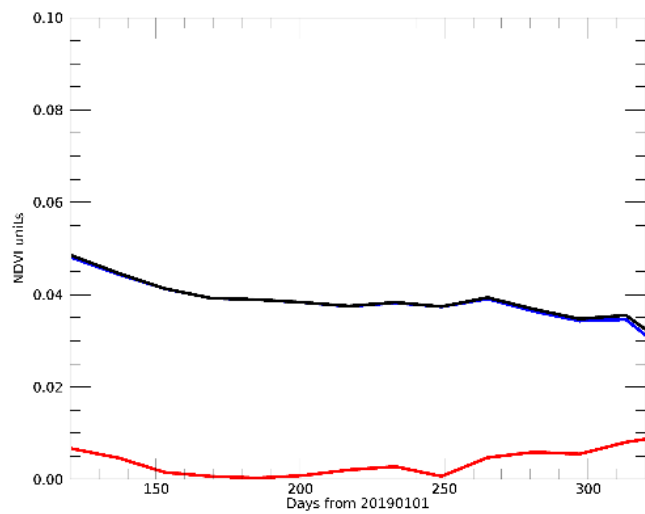
(a)



(b)



(c)



(d)

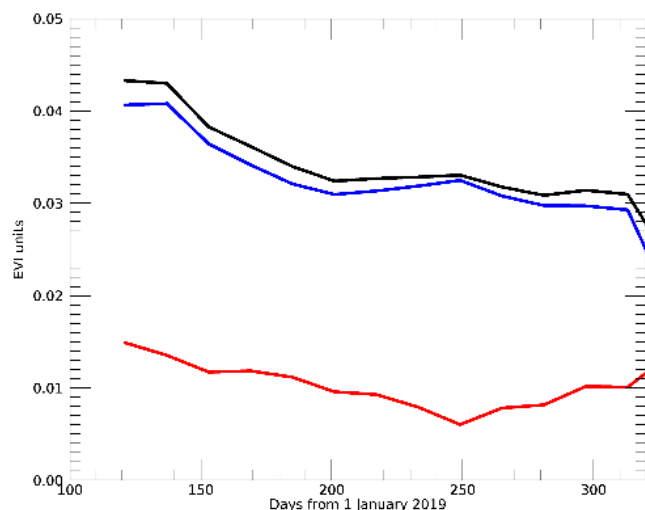


Figure 19: Accuracy (red), precision (blue), and uncertainty (black) statistics for biweekly global NPP VIIRS vs. MODIS vegetation indices. (a) and (b) are stratified by NOAA VI value, with histograms of numbers of pixels shown in gray. (a) TOC NDVI. (b) TOC EVI. Time series are shown in (c) and (d). (c) TOC NDVI. (d) TOC EVI.

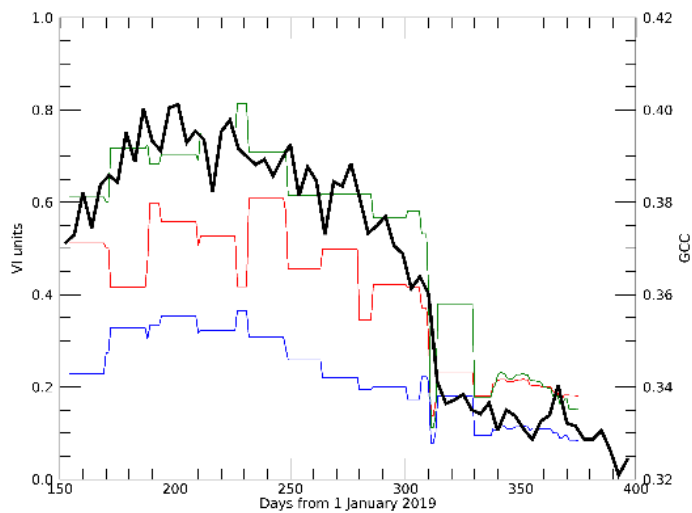
Table 15. Overall statistics for NPP VIIRS vs. MODIS vegetation indices.

	TOC NDVI	TOC EVI
Accuracy	0.0034	0.0107
Precision	0.0382	0.0322
Uncertainty	0.0384	0.0339

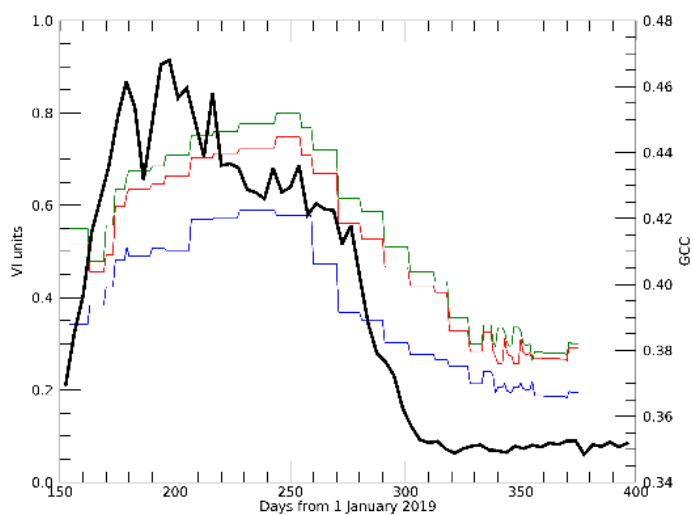
Results of comparison of NOAA20 vegetation indices to PhenoCam GCC values are shown in Figure 20 and Table 16. Figure 20 shows examples of vegetation index versus GCC time series at three sites. These sites are in the Northern Hemisphere and the time period is June-December 2019, so the fact that VIs and GCC all show a decreasing trend is as expected. Table 16 shows Spearman rank correlation coefficients (r_s) between NOAA20 VIIRS global biweekly TOC EVI and the PhenoCam GCCs. There is a wide range of correlation

coefficients, with some lower correlations possibly due to spatial mismatch between the PhenoCam view subset and VIIRS global VI grid cell. The results are consistent with what Brown et al. (2017) found for similar comparisons between PhenoCam GCCs and MERIS TOC NDVIs.

(a)



(b)



(c)

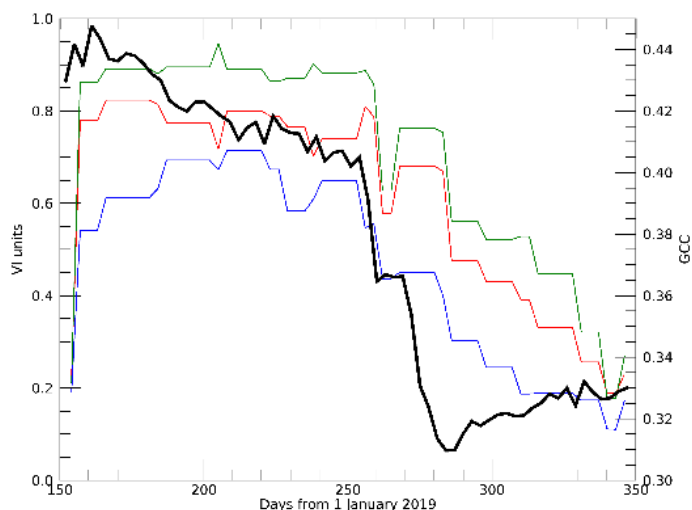


Figure 20: Time series of June- December 2019 biweekly global NOAA20 TOA NDVI (red), TOC NDVI (green), and TOC EVI (blue) compared to PhenoCam GCC (black), for (a) CanadaOBS site, (b) mead2 site, (c) willowcreek site.

Table 16: Spearman rank correlation coefficients between biweekly global NOAA20 TOC NDVI and PhenoCam GCC for June-December 2019

Site	$r_{s_TOC_NDVI}$	Site	$r_{s_TOC_NDVI}$
alligatorriver	0.399	montenegro	0.571
archboldpnot	0.106	morganmonroe2	0.724
burnssagebrush	0.462	NEON_D04_GUAN	0.339
cafcookeastltar01	0.118	NEON_D08_TALL	0.550
canadaOBS	0.849	NEON_D10_ARIK	0.408
dukehw	0.842	NEON_D11_OAES	0.690
jurong	0.667	NEON_D18_TOOL	0.857
luckyhills	0.779	NEON_D19_BONA	0.799
mandani2	0.246	southerngreatplains	0.578
mead2	0.554	tworfta	0.693
monteblanco	0.493	willowcreek	0.696

In summary, comparison of NPP to NOAA20 gridded VI EDRs show that the overall discrepancies between them fall within the specification for the product. In addition, comparison of biweekly global NOAA NPP VIIRS vegetation indices with other global gridded satellite products also shows that the products are consistent to within the VIIRS VI EDR specification. Comparison with PhenoCam GCCs does not yield an exact comparison to VI values, but does show trends generally in the same direction and a degree of correlation consistent with that found with MERIS. No comparison with FLUXNET data was performed for the validated maturity review, but validation against FLUXNET is planned future work.

4. ASSUMPTIONS AND LIMITATIONS

4.1 *Assumptions*

The following assumptions have been made in determining that the VIIRS VI system architecture as designed will meet the requirements.

- VIIRS surface reflectance and TOA reflectance in I1, I2 and M3 bands are available, calibrated and navigated and are not distorted.
- JPSS Risk Reduction Unique Aerosol Optical Depth (JRR-AOD) data are available and the quality of the AOD data are high.
- JPSS Risk Reduction Unique Cloud Mask (JRR-CloudMask) data are available and the quality of the cloud mask data are high.

4.2 *Limitations*

The NVPS VIIRS VI system calculates vegetation index for all areas including snow and high latitude areas. But for the high latitude area in the North Hemisphere in winter, there are no optical observations from the VIIRS sensor due to the lack of sunlight or extremely high solar zenith angle ($>80^\circ$). For pixels in this region, VI is missing.

There are large areas of cloud in the daily reflectance map, so the daily VI products are strongly affected by the presence of cloud.

The VIIRS NDVI and EVI data vary depending on the viewing and illumination geometry due to bidirectional reflectance distribution function (BRDF) effects, particularly over heterogeneous surfaces. There is no angular correction for the VIIRS NDVI and EVI data.

The variation of the atmospheric composition, such as aerosol, affects the quality of the TOA NDVI data. There is no atmospheric correction on the VIIRS TOA NDVI data.

5. LIST OF REFERENCES

- Ahl D. E., S. T. Gower, S. N. Burrows, N. V. Shabanow, R. B. Myneni, and Y. Knyazikhim (2006). Monitoring spring canopy phenology of a deciduous broadleaf forest using MODIS. *Remote Sensing of Environment*, 104, 88–95.
- Anyamba, A., and C. J. Tucker (2005). Analysis of Sahelian vegetation dynamics using NOAA-AVHRR NDVI data from 1981–2003. *Journal of Arid Environments*, 63, 596–614.
- Baret F., O. Hagolle, B. Geiger, P. Bicheron, B. Miras, M. Huc, B. Berthelot, F. Nino, M. Weiss, O. Samain, J. L. Roujean, and M. Leroy (2007). LAI, fAPAR, and fCover CYCLOPES global products derived from VEGETATION – Part 1: Principles of the algorithm *Remote Sensing of Environment*, 110, 275–285.
- Blackburn, A. G. (1998), Quantifying chlorophylls and carotenoids at leaf and canopy scales: An evaluation of some hyperspectral approaches. *Remote Sensing of Environment*, 66, 273–285.
- Boegh, E., H. Soegaard, N. Broge, C. B. Hasager, N. O. Jensen, K. Schelde, K., (2002). Airborne multispectral data for quantifying leaf area index, nitrogen concentration, and photosynthetic efficiency in agriculture. *Remote Sensing of Environment*, 81, 179–193.
- Brown, L. A., J. Dash, B. O. Ogutu, and A. D. Richardson (2017)). On the relationship between continuous measures of canopy greenness derived using near-surface remote sensing and satellite-derived vegetation products. *Agricultural and Forest Meteorology*, 247: 280–292. DOI: [10.1016/j.agrformet.2017.08.012](https://doi.org/10.1016/j.agrformet.2017.08.012)
- Cabral, A., M. J. P. De Vasconcelos, J. M. C. Pereira, E. Bartholomé, and P. Mayaux (2003). Multi-temporal compositing approaches for SPOT-4 VEGETATION. *International Journal of Remote sensing*, 24 (16), 3343–3350.
- Carreiras, J.M B., J. M. C. Pereira, Y. E. Shimabukuro, and D. Stroppiana (2003). Evaluation of compositing algorithms over the Brazilian Amazon using SPOT-4 VEGETATION data. *International Journal of Remote sensing*, 24 (17), 3427–3440.
- Chen, J. M., and J. Cihlar (1996). Retrieving leaf area index of boreal conifer forests using Landsat TM images. *Remote Sensing of Environment*, 55, 153–162.
- Chen, X., L. Vierling, E. Rowell, and T. DeFelice (2004). Using lidar and effective LAI data to evaluate IKONOS and Landsat 7 ETM+ vegetation cover estimates in a ponderosa pine forest. *Remote Sensing of Environment*, 91, 14–26.

- Cihlar, J., D. Manak, and M. D'lorio (1994). Evaluation of compositing algorithms for AVHRR data over land. *IEEE Transactions on Geoscience and Remote Sensing*, 32 (2), 427-437.
- Defries, R. S., and A. S. Belward, (2000). Global and regional land cover characterization from satellite data. *International Journal of Remote Sensing*, 21, 1083-1092.
- Di Bella, C. M., Paruelo, J. M., Becerra, J. E., Bacour, C., & Baret, F. (2004). Effect of senescent leaves on NDVI-based estimates of f APAR: experimental and modelling evidences. *International Journal of Remote Sensing*, 25, 5415-5427.
- Funk, C. and M. E. Budde (2009). Phenologically-tuned MODIS NDVI-based production anomaly estimates for Zimbabwe. *Remote Sensing of Environment*, 113, 115-125.
- Gitelson, A. A., Vina, A., Ciganda, V., Rundquist, C. D., & Arkebauer, J. T. (2005). Remote estimation of canopy chlorophyll content in crops. *Geophysical Research Letters*, 32, L08403. doi:10.1029/2005GL022688.
- Gutman, G. (1991). Vegetation indices from AVHRR: an update and future prospects. *Remote Sensing of Environment*, 35, 121-136.
- Gutman, G., and A. Ignatov (1998). The derivation of the green vegetation fraction from NOAA/AVHRR data for use in numerical weather prediction models. *International Journal of Remote Sensing* 19, 1533-1543.
- Houborg, R., H. Soegaard, and E. Boegh (2007). Combining vegetation index and model inversion methods for the extraction of key vegetation biophysical parameters using Terra and Aqua MODIS reflectance data. *Remote Sensing of Environment*, 106, 39-58.
- Huete, A. R. (1988). A soil-adjusted vegetation index (SAVI). *Remote Sensing of Environment*, 25, 295-309.
- Huete, A. R., G. Hua, J. Qi, A. Chehbouni, and W. J. D. van Leeuwen (1992). Normalization of multidirectional red and NIR reflectances with the SAVI. *Remote Sensing of Environment*, 41, 143-154.
- Huete, A. R., K. Didan, T. Miura, E. P. Rodriguez, X. Gao, and L. G. Ferreira (2002). Overview of the radiometric and biophysical performance of the MODIS vegetation indices. *Remote Sensing of Environment*, 83, 195-213.
- Huete, A. R., K. Didan, Y. E. Shimabukuro, P. Ratana, C. R. Saleska, L. R. Hutya, W. Yang, R. R. Nemani, and R. Myneni, (2006). Amazon rainforests green-up with sunlight in dry season. *Geophysical Research letters*, 33, L06405, doi:10.1029/2005GL025583.

- Jiang, Z., A. R. Huete, J. Chen, Y. Chen, J. Li, G. Yan, and X. Zhang (2006). Analysis of NDVI and scaled difference vegetation index retrievals of vegetation fraction. *Remote Sensing of Environment*, 101, 366-378.
- Jiang, Z., A.R. Huete, K. Didan, T. Miura (2008). Development of a two-band enhanced vegetation index without a blue band. *Remote Sensing of Environment*, 112, 3833–3845.
- Joint Polar Satellite System (JPSS) VIIRS Vegetation Index (VVI) Algorithm Theoretical Basis Document (ATBD), April 22, (2011).
- Kaufman, Y. J., and D. Tanré (1992). Atmospherically resistant vegetation index (ARVI) for EOS-MODIS. *IEEE Transactions on Geoscience and Remote Sensing*, 30, 261-270.
- Liu, H., and A. R. Huete (1995). A feedback based modification of the NDVI to minimize canopy background and atmospheric noise. *IEEE Transactions on Geoscience and Remote Sensing*, 33, 457-465.
- Lunetta, R. S., J. F. Knight, J. Ediriwickrema, J. G. Lyon, and L. D. Worthy (2006). Land-cover change detection using multi-temporal MODIS NDVI data. *Remote Sensing of Environment*, 105, 142-154.
- Miura, T., J. Muratsuchi, and M. Vargas. (2018). Cross-comparison of VIIRS and MODIS vegetation indices using one-year global data. *Remote Sensing*, (in preparation).
- Myneni, B. R., Keeling, D. C., Tucker, J. C., Asrar, G., & Nemani, R. R. (1997a). Increased plant growth in the northern high latitudes from 1981 to 1991. *Nature*, 386(17), 698–702.
- Myneni, B. R., Nemani, R. R., & Running, W. S. (1997b). Estimation of global leaf area and absorbed PAR using radiative transfer models. *IEEE Transactions on Geoscience and Remote Sensing*, 35, 1380–1393.
- Nagler, P. L., Cleverly, J., Glenn, E., Lampkin, D., Huete, A. R., & Wan, Z. (2005). Predicting riparian evapotranspiration from MODIS vegetation indices and meteorological data. *Remote Sensing of Environment*, 94, 17–30.
- NOAA STAR/ OSPO (2018). VIIRS Surface Reflectance External User’s Manual. Version 2.0, July 2018.
- Rahman, A. F., D. A. Sims, V. D. Cordova, and B. Z. El-Masri (2005). Potential of MODIS EVI and surface temperature for directly estimating per-pixel ecosystem C fluxes. *Geophysical Research Letters*, 32, L19404, doi:10.1029/2005GL024127.

- Sims, D. A., A. F. Rahman, V. D. Cordova, B. Z. El-Masri, D. D. Baldocchi, L. B. Flanagan, A. H. Goldstein, D. Y. Hollinger, L. Misson, R. K. Monson, W. C. Oechel, H. P. Schmid, S. C. Wofsy, and L. Xu (2006). On the use of MODIS EVI to assess gross primary productivity of North American ecosystems. *Journal of Geophysical Research*, 111, G04015, doi:10.1029/2006JG000162.
- Sims, D. A., Rahman, A. F., Cordova, V. D., El-Masri, B. Z., Baldocchi, D. D., Bolstad, P. V., et al. (2008). A new model of gross primary productivity for North American ecosystems based solely on the enhanced vegetation index and land surface temperature from MODIS. *Remote Sensing of Environment*, 112, 1633–1646.
- Stoms, D.M., Bueno, M.J., Davis, F.W. (1997). Viewing geometry of AVHRR image composites derived using multiple criteria. *Photogrammetric Engineering & Remote Sensing*, 63 (6), 681-689.
- Suzuki, K., Masuda, K., & Dye, D. G. (2007). Interannual covariability between actual evapotranspiration and PAL and GIMMS NDVIs of northern Asia. *Remote Sensing of Environment*, 106, 387–398.
- Townshend, J. R. G. (1994). Global data sets for land applications from the advanced very high resolution radiometer: An introduction. *International Journal of Remote Sensing*, 15, 3319–3332.
- Tucker, J. C., Fung, I. Y., Keeling, C. D., & Gammon, R. H. (1986). Relationship between atmospheric CO₂ variations and a satellite-derived vegetation index. *Nature*, 319, 195–199.
- van Leeuwen, W.J.D., Huete, A.R., Laing, T.W. (1999). MODIS vegetation index compositing approach: a prototype with AVHRR data. *Remote Sensing of Environment*, 69 (3), 264-280.
- Vargas, M., Miura, T., Shabanov, N., & Kato, A. (2013). An initial assessment of Suomi NPP VIIRS vegetation index EDR. *Journal of Geophysical Research-Atmospheres*, 118, 12301-12316.
- Vargas, M., T. Miura, Z. Jiang, M. Chen, A. Kato, J. Muratsuchi. (2017). NOAA SNPP/JPSS VIIRS vegetation products and algorithm development. *97th AMS Annual Meeting*, 22-26 January 2017, Seattle, WA.
- Wardlow, B. D., Egbert, S. L., & Kastens, J. H. (2007). Analysis of time-series MODIS 250m vegetation index data for crop classification in the U.S. Central Great Plains. *Remote Sensing of Environment*, 108, 290–310.

- Waring, R. H., Coops, N. C., Fan, W., & Nightingale, J. M. (2006). MODIS enhanced vegetation index predicts tree species richness across forested ecoregions in the contiguous U.S.A. *Remote Sensing of Environment*, 103, 218–226.
- Wessels, K. J., S. D. Prince, P. E. Frost, and D. van Zyl (2004). Assessing the effects of human-induced land degradation in the former homelands of northern South Africa with a 1 km AVHRR NDVI time-series. *Remote Sensing of Environment*, 91, 47-67.
- Xiao, X., Hagen, S., Zhang, Q., Keller, M., & Moore, B. (2006). Detecting leaf phenology of seasonally moist tropical forests in South America with multi-temporal MODIS images. *Remote Sensing of Environment*, 103, 465–473.
- Xiao, X., Hollinger, D., Aber, J., Goltz, M., Davidson, E. A., Zhang, Q., et al. (2004). Satellitebased modeling of gross primary production in an evergreen needleleaf forest. *Remote Sensing of Environment*, 89, 519–534.
- Zeng, X., Dichinson, E. R., Walker, A., & Shaikh, M. (2000). Derivation and evaluation of global 1-km fractional vegetation cover data for land modeling. *Journal of Applied Meteorology*, 39, 826–839.
- Zhang, X., A. F. Mark, B. S. Crystal, H. S. Alan, C. F. H. John, F. Gao, C. R. Bradley and A. Huete. (2003). *Remote Sensing of Environment*, 84, 471-475.